Article

Not peer-reviewed version

Plastic Design of Metal Thin-Walled Cross-Sections of Any Shape Under Any Combination of Internal Forces

Antonio Aguero * , Ivan Balaz , Torsten Hoglund , Yvona Kolekova

Posted Date: 6 September 2024

doi: 10.20944/preprints202409.0512.v1

Keywords: plastic design; thin-walled cross-sections; Eurocodes; EN 1993-1-1:2022; EN 1999-1- 1:2023; any cross-section shapes; any combination of internal forces; free available programmes

Preprints.org (www.preprints.org) | NOT PEER-REVIEWED | Posted: 6 September 2024 doi:10.20944/preprints202409.0512.v1

Article

Plastic Design of Metal Thin-Walled Cross-Sections of Any Shape under Any Combination of Internal Forces

Agüero Antonio [1,*], Baláž Ivan [2], Höglund Torsten [3] and Koleková Yvona [4]

[1] Universitat Politècnica de València, c/Camino de Vera s/n, 46022 Valencia, Spain, Dept. of Continuous Medium Mechanics and Theory of Structures; anagra@mes.upv.es
[2] Slovak University of Technology in Bratislava · Faculty of Civil Engineering. Department of Metal and Timber Structures. Bratislava, Slovak Republic; ivan.balaz@stuba.sk
[3] Royal Institute of Technology, KTH. Stockholm, Sweden; torstenh@kth.se
[4] Slovak University of Technology in Bratislava · Faculty of Civil Engineering. Department of Structural Mechanics. Bratislava, Slovak Republic; yvona.kolekova@stuba.sk
* Correspondence: anagra@mes.upv.es

Highlights:

- Practical method for plastic design of metal thin-walled cross-sections. MathCad programmes and free available general programmes for interaction diagrams
- Parametric plastic analysis of cross-sections of any shape under any internal force combinations
- Tables for plastic design in practice of monosymmetrical I-shaped sections, channels and Z-sections
- Background of Eurocode formulae for plastic designs, their drawbacks and correct use
- Simple formulae for plastic designof channel under bending moment and bimoment proposed for Eurocodes

Abstract: The introduction provides an overview of beginning the development of a plastic design of metal thin-walled cross-sections. This large study investigates in detail together 14 steel and four extruded aluminium cross-sections. Six groups of various shaped cross-sections that consist of: four I-shaped doubly symmetric sections (two I-sections, one I-section with lips, one H-section); three monosymmetric sections with axis of symmetry z (monosymmetric I-section, T-section, diamond section); four monosymmetric sections with axis of symmetry y (two channels, channel with inside lips, channel with outside lips); two point symmetric sections (Z-section with and without lips); four asymmetric sections (L-profile, sigma section, two closed sections: oblique and irregular sections; non-warping sections along midline, but with negligible warping along the element's thicknesses: T-section and L-profile are included in the above groups. Four extruded aluminium cross-sections are: I 200a section, diamond section and closed oblique and irregular sections. For all 18 cross-sections, the plastic section moduli of three kinds were calculated: $W_{pl,y,nB}$, $W_{pl,z,nB}$ for bimoment not considered to be constraint; $W_{pl,y}$, $W_{pl,z}$, $W_{pl,w}$for bimoment considered to be restraint; maximum values $W_{pl,y,max}$, $W_{pl,z,max}$, $W_{pl,w,max}$. The values of cross-section plastic resistances N_{pl}, $M_{pl,y,Rd}$, $M_{pl,z,Rd}$ and B_{pl} are also calculated in numerical examples. The values of cross-section properties are calculated in different ways to verify the correctness of the results. The following ways of calculations are used: the rules in Eurocode EN 1993-1-1: 2022; own MathCad programmes; own software. Recommendations for educational institutes and designers in practice are provided, including simple formulae for all the cross-sectional properties for the doubly and monosymmetric I-shaped sections, channels and Z-sections. Formulae are presented in six tables containing formulae in the dimensionless form, which are useful for parametrical studies and formulae for direct designs. The background of the Eurocode rules in EN 1993-1-1: 2022 is explained together with recommendations about how to avoid problems with using them.

Keywords: plastic design; thin-walled cross-sections; Eurocodes; EN 1993-1-1:2022; EN 1999-1-1:2023; any cross-section shapes; any combination of internal forces; free available programmes

1. Introduction

 doi:10.20944/preprints202409.0512.v1

Beginning of "Plastic Design" Development

1914: Gábor von Kazinczy (1889-1964) [1], Royal Joseph Polytechnic in Budapest. Gábor von Kazinczy's most important and most influential achievements were experiments with two 5.6-metre and 6-metre long steel beams embedded in a 1-metre wide concrete slab as part of a floor. Firstly, plastic deformations started to develop at ends, and in the middle before collapse. As a result of measurements and observations, Kazinczy introduced the plastic hinges concept. He published his dissertation entitled "Design of clamped end steel beams with regard to the residual deformations" in 1931. The concepts of plastic hinges and the plastic failure mechanism that he developed are very important in the theory of plasticity.

1917: Nicolaas Christiaan Kist (1867-1941) [2]. He studied civil engineering at the Polytechnic University in Delft. With his ideas, Kist laid the foundation for the theory of plasticity. Another contribution by Kist was the so-called "plastic hinge theory" regarding the loading of beam systems, drawn up in 1916. He explained the same plastic hinges concept as Kazinczy and published it in 1930.

1928: Hermann Maier-Leibnitz (1885-1962) [3-5]. In 1917, he received his doctorate in engineering from the Technical University of Stuttgart. Two years later, at the age of just 34, he became professor of Statics in iron and industrial construction at the Stuttgart University of Technology. He is considered one of the founders of the load-bearing method and worked with Gábor von Kazinczy.

1932: Hans Heinrich Bleich (1909-1985) [6]. He studied at Vienna's Technical University, where he obtained a civil engineering degree in 1931 and a doctor of science degree in engineering in 1934. In 1939 he moved to London and to the USA in 1945. In 1947, Bleich joined the Faculty of Columbia University's School of Engineering as a lecturer. He was named professor of civil engineering in 1952 and the Director of the Guggenheim Institute of Air Flight Structures in 1954. He retired from Columbia University in 1975.

1936: John Fleetwood Baker (1901-1985) [7]. He was educated at Rossall School and Clare College, Cambridge. In 1933, Baker became Professor of Engineering at Bristol University. He developed the plastic theory of design, a revolutionary method of the design of steel structures, which gives a lower bound on the collapse load. During his time at Cambridge, the theory of plasticity was used to design the new Baker Building of the department, and it was the first building in the world designed by this method.

Figure 1. Pioneers in plastic design development. From the left: Gábor von Kazinczy [1], Nicolaas Christiaan Kist [2], Hermann Maier-Leibnitz [3], Hans Heinrich Bleich [6] and John Fleetwood Baker [7].

A considerable amount of research has been conducted on the ultimate strength of steel structures since 1930 [8]. All these studies have revealed possibilities for using plastic (maximum) strength as a basis for structural design. Many investigators have contributed to application of plastic

Preprints.org (www.preprints.org) | NOT PEER-REVIEWED | Posted: 6 September 2024 doi:10.20944/preprints202409.0512.v1

analysis to structural design. Some of them from the 1935-1959 period are referred to in chronological order in [8 – 55]. The list of publications also contains important Russian publications. The French contribution appears in [56, 57] and the Czechoslovak one in [58].

The capacity of structural steel to deform plastically allows an indeterminate structure to draw upon the reserve strength of its less heavily stressed portions. By the plastic analysis, engineers are able to determine a structure's true load-carrying capacity.

The plastic design has an appeal for its simplicity. Most of the time-consuming analysis of necessary equations for an elastic solution is eliminated. The "imperfections" that affect a structure's elastic limit strength (sinking of supports, differences in the flexibility of connections, residual stresses) have little or no effect on the maximum plastic strength.

Plastic design promises to produce substantial savings through the more economic and efficient use of steel, as well as savings in design office times.

Plastic design will not replace all other design procedures because, in some instances, criteria other than the maximum plastic strength (i.e. fatigue, instability, limiting deflection, etc.) may actually constitute the basis design. In ordinary building constructions, however, this is not usually the case. Therefore, plastic design is expected to be considerably applied, particularly in continuous beams, industrial frames, and also in tier buildings. It has been reported that until 1955, some 175 industrial frames have been designed in England by the plastic method, along with a school building and five-story office building.

Important theoretical results that relate the plastic resistance of thin-walled cross-sections under combinations of internal forces have been achieved in the last few years by Kindmann [59, 60], Osterrieder [61] and Vayas [62, 63].

The formulae for the plastic design of thin-walled members can be found in modern standards EN 1993 and EN 1999, second-generation Eurocodes, and in the Slovak National Annexe [64] to EN 1993-1-1:2022 [65].

2. Plastic Design in Metal Eurocodes EN 1993-1-1:2022 [65] and EN 1999-1-1:2023 [67]

2.1. Advantages of a Plastic Analysis and Assumptions for Plastic Analysis Applications

The calculation of metal (steel, aluminium) structures according to the theory of plasticity has several advantages, of which at least the four most important ones should be mentioned. It:

a) fully expresses structures' actual behaviour;

b) allows the same safely for a structure and its elements to be attained;

c) the analysis of current structures is often simplified;

d) it is a source of substantial material and cost economies.

A summary of important assumptions for using plastic design:

a) steel and aluminium are regarded as ideal elastoplastic materials, the behaviour of which is described by the idealised stress-strain diagram quite accurately (see Figs. 2, 20 for steel and Figure 19 for aluminium);

b) the material behaves identically in tension and simple compression;

c) the plastic resistance of the structural member at the cross-sections with non-uniform distribution of longitudinal strains is exhausted due to the formation of plastic hinges, which are not capable of resisting any further increase in load;

d) the deformations of structures up to the plastic load-bearing capacity limit are so small that the equilibrium of forces can be investigated for an undeformed structure. The expressions for virtual work can also be formulated with the assumption of small deformations;

e) the longitudinal strains of cross-sections are distributed linearly in cross-section elements. Vlasov`s hypothesis about the non-deforming shape of the cross-section is adopted;

f) a complex stress state of Huber-Mises-Hencky`s condition is usually applied as a condition of plasticity;

g) when the plastic load-bearing capacity or the deflections of statically indeterminate structures are being determined, it is assumed that plastic strains concentrate on the most highly stressed cross-sections: plastic hinges. After the hinge mechanism forms, the curvature of the elements between hinges is assumed to remain unchanged;

h) random imperfections are not taken into account;

Preprints.org (www.preprints.org) | NOT PEER-REVIEWED | Posted: 6 September 2024 doi:10.20944/preprints202409.0512.v1

i) failure due to the local and global instability of members is prevented by structural measures;

j) structural connections are rigid to the extent that they are capable of transferring redistributed effects.

The clauses of Eurocodes EN 1993-1-1:2022 [65] and EN 1999-1-1:2023 [67], which regulate the exploitation of the plastic characteristics of steel and aluminium, shall be respected, in addition to the above enumerated fundamental assumptions.

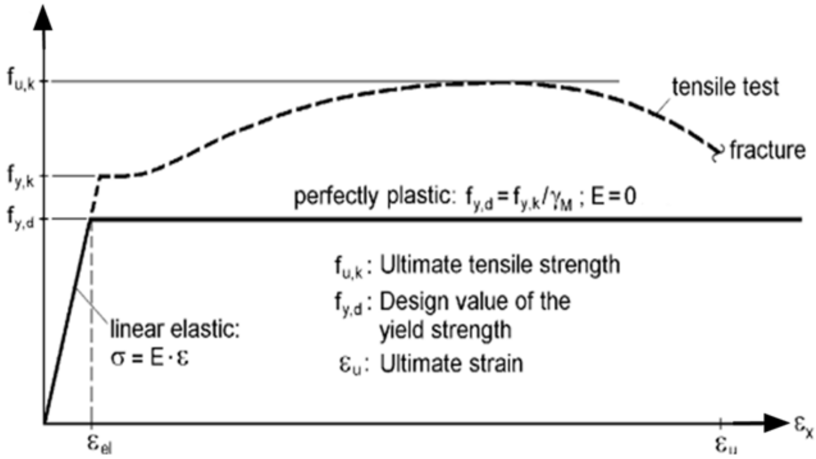

S235: $\boldsymbol{\varepsilon_{el} = \varepsilon_y = f_y / E = 235/21000 = 0.00112}$ $\boldsymbol{\varepsilon_u \geq 0.15}$

S355: $\boldsymbol{\varepsilon_{el} = \varepsilon_y = f_y / E = 355/21000 = 0.0017}$ $\boldsymbol{\varepsilon_u \geq 0.15}$

Figure 2. Assumptions for plastic steel behaviour: $f_u/f_y \geq 1.10$, $\varepsilon_u \geq 15\%$

The authors know that: a) for Class 1 and 2 sections, plastic design may be applied; b) for Class 1, 2 and 3 sections, elastic design can be used; c) for Class 4 sections, elastic design shall be used for effective cross-sections. Nevertheless, in this paper the properties of cross-sections that are not Class 1 or 2 are also calculated to show the used software's ability to investigate any complex shape of cross-sections.

2.2. EN 1993-1-1:2022 [65]

This Eurocode defines the following minimum ductility requirements for a global plastic analysis of steel structures:

a) the ultimate tensile strength to yield strength ratio, $f_u/f_y \geq 1.10$,

b) elongation at failure no less than $\varepsilon_u \geq 15\%$.

NOTE: symbol ε_u is used in EN 1993-1-1:2005 [66] for something else: ultimate strain ε_u corresponds to ultimate strength f_u.

The steels that meet one of the grades up to, including S700, are listed in Table 5.1 and Table 5.2 in [65], and can be assumed to satisfy the minimum ductility requirements for a global plastic analysis. The global plastic analysis allows for materials' non-linearity effects when calculating a structural system's action effects. Behaviour should be modelled by either of these two methods: a) the plastic hinge method or b) the plastic zone method. The global plastic analysis can be used if sufficient lateral restraint is provided in the vicinity of the sections where a plastic hinge or a plastic zone can develop under the design loads.

For the determination of its plastic resistance, a cross-section should be classified according to one of the two following classes: a) the Class 1 cross-sections are those that can form a plastic hinge with the rotation capacity required from the global plastic analysis without reducing resistance; b) the Class 2 cross-sections are those that can develop their plastic bending moment resistance, but they have limited rotation capacity because of local buckling. The maximum width-to-thickness ratios for the Class 1 and 2 compression parts should be obtained from Table 7.3 to Table 7.5 [65]. The cross-section requirements for the global plastic analysis are found in Clause 7.6 [65].

Preprints.org (www.preprints.org) | NOT PEER-REVIEWED | Posted: 6 September 2024 doi:10.20944/preprints202409.0512.v1

Design according to plastic cross-section resistance should be carried out by establishing a stress distribution that is in equilibrium with internal forces without exceeding yield strength. This stress distribution should be compatible with the associated plastic deformations.

The plastic cross-section resistances of the different shapes to a single axial force, bending moment, shear force, bimoment to the combined shear force with Saint-Venant torsional and warping torsional moment, combined bending with bimoment, combined bending with shear and combined bending with axial force, are defined in Clause 8.2 [65].

2.3. EN 1999-1-1:2023 [67]

The characteristic values for the heat-affected zone (0.2 % proof strength, $f_{\mathrm{o,haz}}$ and ultimate tensile strength, $f_{\mathrm{u,haz}}$), reduction factors $\rho_{\mathrm{o,haz}}$ and $\rho_{\mathrm{u,haz}}$ (see 8.1.6), buckling classes A, B, C (used in 8.1.4 and 8.3.1) and exponent n_{p} in the Ramberg-Osgood formula for plastic resistance, should be taken from Tables 5.3 to 5.7 [67].

The global plastic analysis can be used only where the structure has sufficient rotation capacity at the actual location of the plastic hinge, regardless of this being in members or joints. The member should satisfy the requirements specified in 7.4.3. Where a plastic hinge occurs at a joint, the joint shall either have sufficient strength to ensure that the hinge remains in the member or be able to sustain plastic resistance for sufficient rotation. When a plastic hinge occurs on a beam that is asymmetrically perpendicular to the plane of bending (e.g., a channel beam in y-axis bending), the beam should be prevented from rotation occurring at the load application points and at supports. Information on rotation capacity is provided in Annexe L [67]. Only certain alloys have the required ductility to allow sufficient rotation capacity; see K.3 [67]. The global plastic analysis should not be used for beams with transverse welds on the tension side of the member at the plastic hinge locations, except for structures of alloys in 5xxx in temper O or H111, and welded with proper welding metal, because it is documented that the properties in HAZ and the welding zone are no less than in the parent material. Guidance for the global plastic analysis of beams comes in Annexe K [67]. The global plastic should only be used when members' stability can be assured; see 8.3 [67].

The plastic limit state is related to the section's strength, evaluated by assuming perfectly plastic behaviour for a material with a limit value that equals the conventional limit of elasticity f_{o}, without hardening. Global non-linear and rigid plastic analyses can be performed when all the cross-sections where plastic hinges take place are of Class 1 or 2. Cross-sections should be classified depending on their local buckling resistance and rotation capacity. The Class 1 cross-sections whose plastic moment resistance develops by forming a plastic hinge with the rotation capacity required for the plastic analysis. The Class 2 cross-sections are those whose plastic moment resistance develops, but they have limited rotation capacity because of local buckling. The effective plastic modulus of gross cross-section $W_{\mathrm{pl,haz}}$ obtained using reduced thickness $\rho_{\mathrm{o,haz}}t$ for the HAZ material (see 8.2.5.2), appears in Table 4 [60]. When the global plastic analysis is used for the ultimate limit state, the effects of plastic redistribution of the forces and moments at the serviceability limit state should be considered. The following assumptions for material behaviour can be used: the true stress-strain curve represented through the Ramberg-Osgood law (Formula (F.14) [67]) with exponent $n = n_{\mathrm{p}}$ from Table 5.3 and Table 5.4 [67]. This curve should be utilised if plastic resistance should be found.

2.4. The Plastic Section Modulus [67]

The cross-section is divided into n parts numbered as shown in Figure 3. The following procedure can be used for plastic section modulus $W_{\mathrm{pl,y}}$:

1. Add an extra node in the part, which will be crossed by the plastic neutral axis (PNA);
2. Define the PNA so that the areas above and below the PNA are the same (= $A/2$);
3. Replace thickness t_{i} below the PNA with negative value -t_{i};

4. Plastic section modulus $W_{\mathrm{pl,y}}$ is then given by Formula (1).

$$W_{\mathrm{pl,y}} = \sum_{i=1}^{n} 0.5 t_i (z_i + z_{i-1}) \sqrt{(z_i - z_{i-1})^2 + (y_i - y_{i-1})^2} \qquad (1)$$

For plastic section modulus $W_{\mathrm{pl},z}$, change y and z, and add a vertical PNA line and extra node(s) on this line.

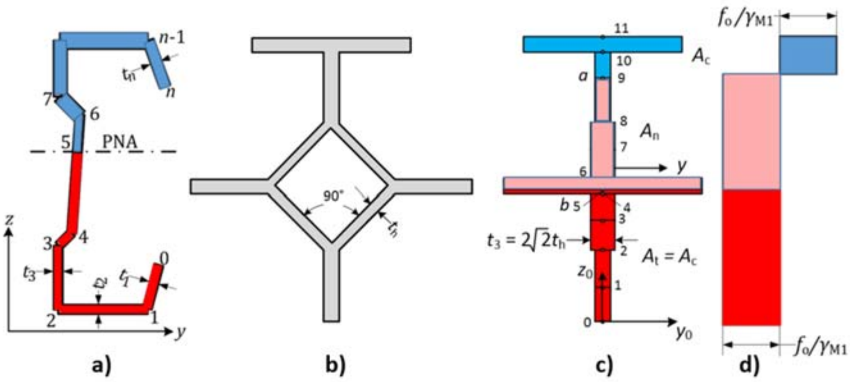

Figure 3. Cross-section subdivision parts: a) open cross-section with an extra node (5) and a plastic neutral axis; PNA; b) cross-section with inclined parts and a diamond shape; c) compressed cross-section equivalent to (b), where the thickness of inclined parts is measured horizontally; d) stresses where parts 6 to 9 give axial force, and 1 to 5 (A_t) and 6 to 11 (A_c) give the moment. $\boldsymbol{f_o}$ is the characteristic value of 0.2% proof strength. $\boldsymbol{\gamma_{M1}}$=1.1 in [67].

2.5. Plastic Interaction Formula

The cross-section is divided into parts as numbered in Figure 3. A cross-section with more than one web (Figure 3b) can be concentrated as in Figure 3c. The following procedure may be used to find a point on the interaction diagram for the axial force *versus* the bending moment:

1. Choose a node a (= 9 in Figure 3c) above which there are compression stresses;
2. Calculate area Ac above this node a;
3. Add an extra node b (= 5 in Figure 3c) on the tension side, placed in such a way that area At below this node is the same as Ac;
4. Set thickness to – ti for parts 1 to b and to 0 for parts b+1 to a;
5. Calculate the reduced plastic section modulus with Formula (1);
6. Calculate area An = A - 2Ac;
7. A point on the interaction diagram is now given by MRd = Wpl,y fo/γM1 and NRd = An fo/γM1;
8. Repeat the procedure for the other nodes a;
9. If the bending moment resistance is searched for a specific axial force, then node a should be chosen so that Ac = 0.5(A - NRd /(fo /γM1)).

Eurocode EN 1999-1-1:2007 [68] offered in the formulae of informative Annexes C and Jto calculate the: a) cross-section constants for thin-walled open cross-sections (C.1, J.1); b) cross-section constants for open cross-sections with branches (C.2, J.2); c) torsion constant and shear centre of cross-sections with a closed part (C3, J.3). EN 1999-1-1:2023 [67] contains in informative Annexe G the same formulae as in the 2007 edition [68], but also the formulae for calculating the shear area (G.9) [67], the plastic section modulus and the interaction formula.

 doi:10.20944/preprints202409.0512.v1

The formulae in the above-mentioned Eurocodes appear in the form of formulae, and are especially convenient for use in the MathCad software and similar programmes where formulae are presented in the same format as formulae in textbooks and codes. This also helps MathCad software users, but formulae may be evaluated by any other programme.

Formulations are especially convenient for cold-formed sections where thickness is the same for all the cross-section elements. These are automatically defined from nodes.

As elements are given with the midline dimension and thicknesses, some errors may occur in corners depending on how corners are modelled. If they are modelled with one node, then there will be some overlapping of the area (red) and missing area (white) according to Figure 4a. The cross-section area will always be correct, but there will be a small error in I_y, I_z and so on, because area $t/2 \times t/2$ (red in the Figure 4a) will have a small error in the distance to the coordinate axis. This error is usually negligible in corners, but the error may be notable in the sections with branches because the area is doubled in the overlapping area (red in Figure 4d). These errors can be overcome if corners are modelled with two nodes according to Figure 4b and 4c with an element with thickness 0 between them.

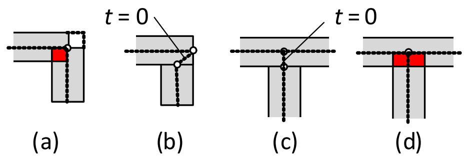

Figure 4. Nodes in corners and in the connections between elements.

Examples of the numbering nodes in the MathCad formulae [67] are given in Figure 5 for the cross-sections without branching and in Figure 6 for the cross-sections with branches.

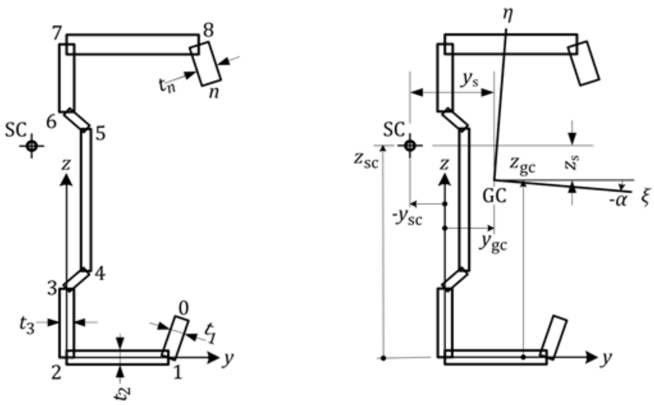

Figure 5. – Numbering of nodes in a cross-section without branching.

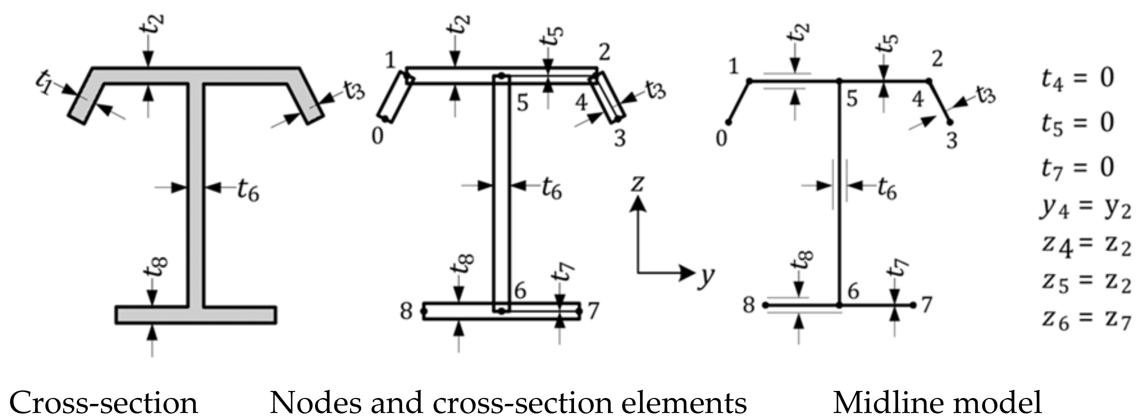

Figure 6. Nodes and parts in a cross-section with branches.

 doi:10.20944/preprints202409.0512.v1

a) Divide the cross-section into n parts. Number parts 1 to n: Insert nodes between parts. Number nodes 0 to n. Part i is then defined by nodes i - 1 and i. Give nodes, co-ordinates and (effective) thickness. j = 0 …n are nodes and, i = 1 … n are cross-section parts. Note that y - z is an arbitrary coordinate system and the origin is not usually at the center of gravity. Here the principal axes are denoted as ξ and η.

b) Calculate the following geometrical magnitudes:

Area of the cross-section parts by Formula (2) as:

$$\Delta A_i = t_i \sqrt{\left(y_i - y_{i-1}\right)^2 + \left(z_i - z_{i-1}\right)^2} \tag{2}$$

Cross-section area by Formula (3):

$$A = \sum_{i=1}^{n} \Delta A_i \tag{3}$$

The first moment of the area in respect to the y-y-axis and the coordinate of the centroid by Formula (4):

$$S_{y0} = \sum_{i=1}^{n} \left(z_i + z_{i-1}\right) \frac{\Delta A_i}{2} \qquad z_{gc} = \frac{S_{y0}}{A} \tag{4}$$

The moment of inertia in relation to the original y-y-axis and the new y-y-axis through centroid by Formula (5):

$$I_{y0} = \sum_{i=1}^{n} \left((z_i)^2 + (z_{i-1})^2 + z_i z_{i-1}\right) \frac{\Delta A_i}{3} \qquad I_y = I_{y0} - A z_{gc}^2 \tag{5}$$

The first moment of area in relation to the z-axis and the gravity centre by Formula (6):

$$S_{z0} = \sum_{i=1}^{n} \left(y_i + y_{i-1}\right) \frac{\Delta A_i}{2} \qquad y_{gc} = \frac{S_{z0}}{A} \tag{6}$$

The moment of inertia in relation to the original z-axis and the new z-axis through centroid by Eq. (7)

$$I_{z0} = \sum_{i=1}^{n} \left((y_i)^2 + (y_{i-1})^2 + y_i y_{i-1}\right) \frac{\Delta A_i}{3} \qquad I_z = I_{z0} - A y_{gc}^2 \tag{7}$$

Product moment of area with respect of original y- and z-axis and new axes through centroid by Formula (8) as

$$I_{yz0} = \sum_{i=1}^{n} \left(2y_{i-1} z_{i-1} + 2y_i z_i + y_{i-1} z_i + y_i z_{i-1}\right) \frac{\Delta A_i}{6}, \quad I_{yz} = I_{yz0} - \frac{S_{y0} S_{z0}}{A} \tag{8}$$

The principal axis by Formulae (9), (10) and (11):

$$\alpha = \frac{1}{2} \arctan\left(\frac{2I_{yz}}{I_z - I_y}\right) \text{ if } I_z - I_y \neq 0\text{, otherwise } \alpha = 0 \tag{9}$$

$$I_\xi = \frac{1}{2}\left(I_y + I_z + \sqrt{(I_y - I_z)^2 + 4(I_{yz})^2}\right) \tag{10}$$

$$I_\eta = \frac{1}{2}\left(I_y + I_z - \sqrt{(I_y - I_z)^2 + 4(I_{yz})^2}\right) \tag{11}$$

The sectorial coordinates by Formula (12)

$$\omega_0 = 0 \qquad \omega_{0_i} = y_{i-1} z_i - y_i z_{i-1}, \qquad \omega_i = \omega_{i-1} + \omega_{0_i} \tag{12}$$

The mean of the sectorial coordinate by Formula (13):

$$I_\omega = \sum_{i=1}^{n} \left(\omega_{i-1} + \omega_i\right) \frac{\Delta A_i}{2} \qquad \omega_{mean} = \frac{I_\omega}{A} \tag{13}$$

The sectorial constants by Formulae (14), (15) and (16):

Preprints.org (www.preprints.org) | NOT PEER-REVIEWED | Posted: 6 September 2024 doi:10.20944/preprints202409.0512.v1

$$I_{y\omega 0}=\sum_{i=1}^{n}\left(2y_{i-1}\omega_{i-1}+2y_i\omega_i+y_{i-1}\omega_i+y_i\omega_{i-1}\right)\frac{\Delta A_i}{6},\quad I_{y\omega}=I_{y\omega 0}-\frac{S_{z0}I_{\omega}}{A} \tag{14}$$

$$I_{z\omega 0}=\sum_{i=1}^{n}\left(2z_{i-1}\omega_{i-1}+2z_i\omega_i+z_{i-1}\omega_i+z_i\omega_{i-1}\right)\frac{\Delta A_i}{6},\quad I_{z\omega}=I_{z\omega 0}-\frac{S_{y0}I_{\omega}}{A} \tag{15}$$

$$I_{\omega\omega 0}=\sum_{i=1}^{n}\left((\omega_i)^2+(\omega_{i-1})^2+\omega_i\omega_{i-1}\right)\frac{\Delta A_i}{3},\qquad I_{\omega\omega}=I_{\omega\omega 0}-\frac{I_{\omega}^2}{A} \tag{16}$$

The shear centre by Formula (17):

$$y_{sc}=\frac{I_{z\omega}I_z-I_{y\omega}I_{yz}}{I_yI_z-I_{yz}^2},\quad z_{sc}=\frac{-I_{y\omega}I_y+I_{z\omega}I_{yz}}{I_yI_z-I_{yz}^2},\quad \left(I_yI_z-I_{yz}^2\neq 0\right) \tag{17}$$

The warping constant by Formula (18):

$$I_w=I_{\omega\omega}+z_{sc}\cdot I_{y\omega}-y_{sc}\cdot I_{z\omega}, \tag{18}$$

The torsion constants by Formula (19):

$$I_t=\sum_{i=1}^{n}\left(t_i\right)^2\frac{\Delta A_i}{3}\qquad W_t=\frac{I_t}{\max(t)} \tag{19}$$

The sectorial coordinate in relation to the shear centre by Formula (20):

$$\omega_{s_j}=\omega_j-\omega_{mean}+z_{sc}\left(y_j-y_{gc}\right)-y_{sc}\left(z_j-z_{gc}\right) \tag{20}$$

The maximum sectorial coordinate and warping modulus by Formula (21):

$$\omega_{max}=max(|\omega_s|)\qquad W_w=\frac{I_w}{\omega_{max}} \tag{21}$$

The distance between the shear centre and the centroid by Formula (22):

$$y_s=y_{sc}-y_{gc},\qquad z_s=z_{sc}-z_{gc} \tag{22}$$

The polar moment of inertia in relation to the shear centre by Formula (23):

$$I_p=I_y+I_z+A\left(y_s^2+z_s^2\right) \tag{23}$$

Non-symmetry factors z_j and y_j according to Annexe I [60] by Formulae (24) and (25):

$$z_j=z_s-\frac{0.5}{I_y}\sum_{i=1}^{n}\left[(z_{c_i})^3+z_{c_i}\left(\frac{(z_i-z_{i-1})^2}{4}+y_{c_i}{}^2+\frac{(y_i-y_{i-1})^2}{12}\right)+y_{c_i}\frac{\left(y_i-y_{i-1}\right)\left(z_i-z_{i-1}\right)}{6}\right]\cdot\Delta A_i \tag{24}$$

$$y_j=y_s-\frac{0.5}{I_z}\sum_{i=1}^{n}\left[(y_{c_i})^3+y_{c_i}\left(\frac{(y_i-y_{i-1})^2}{4}+z_{c_i}{}^2+\frac{(z_i-z_{i-1})^2}{12}\right)+z_{c_i}\frac{\left(z_i-z_{i-1}\right)\left(y_i-y_{i-1}\right)}{6}\right]\cdot\Delta A_i \tag{25}$$

where the coordinates for the centre of the cross-section parts in relation to the centroid are given by Formula (26):

$$y_{c_i}=\frac{y_i+y_{i-1}}{2}-y_{gc}\qquad z_{c_i}=\frac{z_i+z_{i-1}}{2}-z_{gc} \tag{26}$$

NOTE: $z_j=0$ $\left(y_j=0\right)$ for the cross-sections with the *y*-*y*-axis (*z*-*z*-axis) being the axis of symmetry (Figure 5).

 doi:10.20944/preprints202409.0512.v1

In the cross-sections with branches, the formulae in (22)-(26) can be used. However, follow the branching back (with thickness $t = 0$) to the next part with thickness $t \neq 0$; see branches 3 - 4 - 5 and 6 - 7 in Figure 6.

3. Basis of the Theory

The static or lower bound theorem is applied. The equilibrium and plastic condition are satisfied so that the plastification factor equals or is smaller than the plastic one.

Nomenclature of the plastic section properties:

1- Without taking the bimoment as a constraint: $W_{pl,zy,nb}$, $W_{pl,z,nB}$.

2- Taking the bimoment as a constraint: $W_{pl,y}$, $W_{pl,z}$, $W_{pl,w}$.

3- Maximum: $W_{pl,y,max}$, $W_{pl,z,max}$, $W_{pl,w,max}$.

The interaction equations for the plastic resistance of cross-sections $N_{pl,Rd}$, $M_{pl,y,Rd}$, $M_{pl,z,Rd}$ Eurocode 3 are obtained without considering that bimoment B_{Ed} is a constraint.

The following method 1 was implemented in two computer programmes.

The software can be found in the following blog:

https://antonioagueroramonllin.blogs.upv.es/

1- thinwallsectiongeneral to compute values when taking the bimoment as a constraint and maximum values:

https://laboratoriosvirtuales.upv.es/webapps/thinwallsectiongeneral.html

2- thinwallsectionopenclosed to compute values without considering the bimoment a constraint:

https://labmatlab-was.upv.es/webapps/home/thinwallsectionopenclosed.html

3.1. Method 1 to Obtain Plastic Parameters

The following tables explain how to obtain the section properties. The obtained values are divided by f_y. The cross-section is divided into n fibers of Area A(i), coordinates y(i), z(i), unit warping w(i). The normal stress σ(i) values at each fibre are optimised to maximise the different linear functions in the tables with the corresponding linear constraints. This problem can be solved using simplex (linear programming).

Table 1. Case 1: Computation of plastic parameters without considering bimoment B_{Ed} to be a constraint.

Maximise	$N = \sum_{i=1}^{n} A(i)\sigma(i)$	$My = \sum_{i=1}^{n} z(i)A(i)\sigma(i)$	$Mz = -\sum_{i=1}^{n} y(i)A(i)\sigma(i)$
Constraints	$My = \sum_{i=1}^{n} z(i)A(i)\sigma(i) = 0$	$N = \sum_{i=1}^{n} A(i)\sigma(i) = 0$	$My = \sum_{i=1}^{n} z(i)A(i)\sigma(i) = 0$
	$Mz = -\sum_{i=1}^{n} y(i)A(i)\sigma(i) = 0$	$Mz = -\sum_{i=1}^{n} y(i)A(i)\sigma(i) = 0$	$N = \sum_{i=1}^{n} A(i)\sigma(i) = 0$
	$-fy < \sigma(i) < fy$		

Table 2. Case 2: Computation of plastic parameters by considering bimoment B_{Ed} to be a constraint.

Maximise	$N = \sum_{i=1}^{n} A(i)\sigma(i)$	$My = \sum_{i=1}^{n} z(i)A(i)\sigma(i)$	$Mz = -\sum_{i=1}^{n} y(i)A(i)\sigma(i)$	$B = \sum_{i=1}^{n} \omega(i)A(i)\sigma(i)$

 doi:10.20944/preprints202409.0512.v1

Constraints	$My = \sum_{i=1}^{n} z(i)A(i)\sigma(i) = 0$	$N = \sum_{i=1}^{n} A(i)\sigma(i) = 0$	$My = \sum_{i=1}^{n} z(i)A(i)\sigma(i) = 0$	$My = \sum_{i=1}^{n} z(i)A(i)\sigma(i) = 0$
	$Mz = -\sum_{i=1}^{n} y(i)A(i)\sigma(i) = 0$	$Mz = -\sum_{i=1}^{n} y(i)A(i)\sigma(i) = 0$	$N = \sum_{i=1}^{n} A(i)\sigma(i) = 0$	$Mz = -\sum_{i=1}^{n} y(i)A(i)\sigma(i) = 0$
	$B = \sum_{i=1}^{n} \omega(i)A(i)\sigma(i) = 0$	$B = \sum_{i=1}^{n} \omega(i)A(i)\sigma(i) = 0$	$B = \sum_{i=1}^{n} \omega(i)A(i)\sigma(i) = 0$	$N = \sum_{i=1}^{n} A(i)\sigma(i) = 0$
	$-fy < \sigma(i) < fy$			

Table 3. Case 3: Computation of plastic parameters' maximum:.

	N	My	Mz	B
Maximise	$= \sum_{i=1}^{n} A(i)\sigma(i)$	$= \sum_{i=1}^{n} z(i)A(i)\sigma(i)$	$= -\sum_{i=1}^{n} y(i)A(i)\sigma(i)$	$= \sum_{i=1}^{n} \omega(i)A(i)\sigma(i)$
Constraints	$-fy < \sigma(i) < fy$			

3.2. Method 1 to Obtain the Interaction Diagram

In order to obtain the interaction diagram, N, M_y, M_z, plastification factor ξ (the factor by which internal forces must be multiplied to reach a cross-section's plastic resistance) can be obtained for each combination for N_1, M_{y1}, M_{z1} and for 2 N_1, M_{y1}, M_{z1}, B_1 by applying the statics or the lower bound theorem:

Table 4. Computation of plastic factor ξ to plot the interaction diagram.

	Case 1: without considering bimoment B to be a constraint.	Case 2: considering bimoment B to be a constraint
Maximise	ξ	ξ
constraint	$N = \sum_{i=1}^{n} A(i)\sigma(i) = \xi N1$	$N = \sum_{i=1}^{n} A(i)\sigma(i) = \xi N1$
	$My = \sum_{i=1}^{n} z(i)A(i)\sigma(i) = \xi My1$	$My = \sum_{i=1}^{n} z(i)A(i)\sigma(i) = \xi My1$
	$Mz = -\sum_{i=1}^{n} y(i)A(i)\sigma(i) = \xi Mz1$	$Mz = -\sum_{i=1}^{n} y(i)A(i)\sigma(i) = \xi Mz1$
	–	$B = \sum_{i=1}^{n} \omega(i)A(i)\sigma(i) = \xi B1$
	$-fy < \sigma(i) < fy$	

Preprints.org (www.preprints.org) | NOT PEER-REVIEWED | Posted: 6 September 2024 doi:10.20944/preprints202409.0512.v1

4. Numerical Results. Comparisons of the Results of Various Calculation Ways

The study comprises investigating 10 thin-walled profiles (found in Table 5) with their dimensions, plus four other hin-walled cross-sections called diamond section (Figures 3b and c), oblique section (Figure 7a), irregular section (Figure 7b) and sigma section (Figures 5 and 7c).

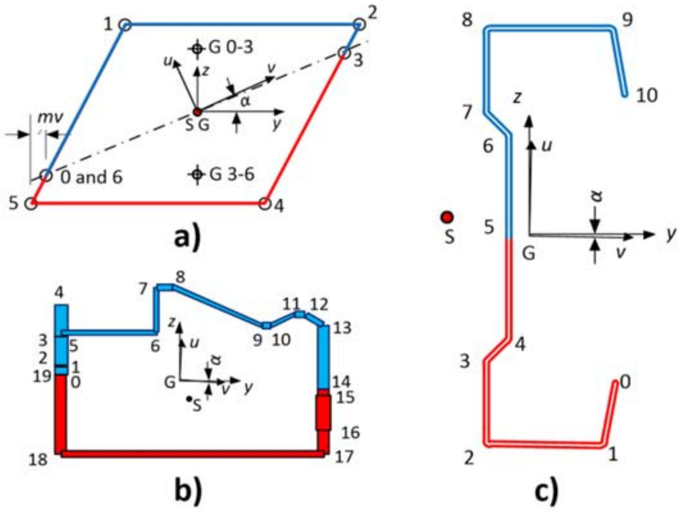

Figure 7. Non-standard cross-sections: a) oblique section, b) irregular section and c) sigma section.

The dimensions of the diamond section (Figure 3c) appear in Table 6, those of the oblique section (Figure 7a) are in Table 7, those of the irregular section (Figure 7b) in Table 8 and Table 9 contains those of the sigma section (Figure 7c).

Table 5. Midline dimensions and thicknesses of the investigated cross-sections [67].

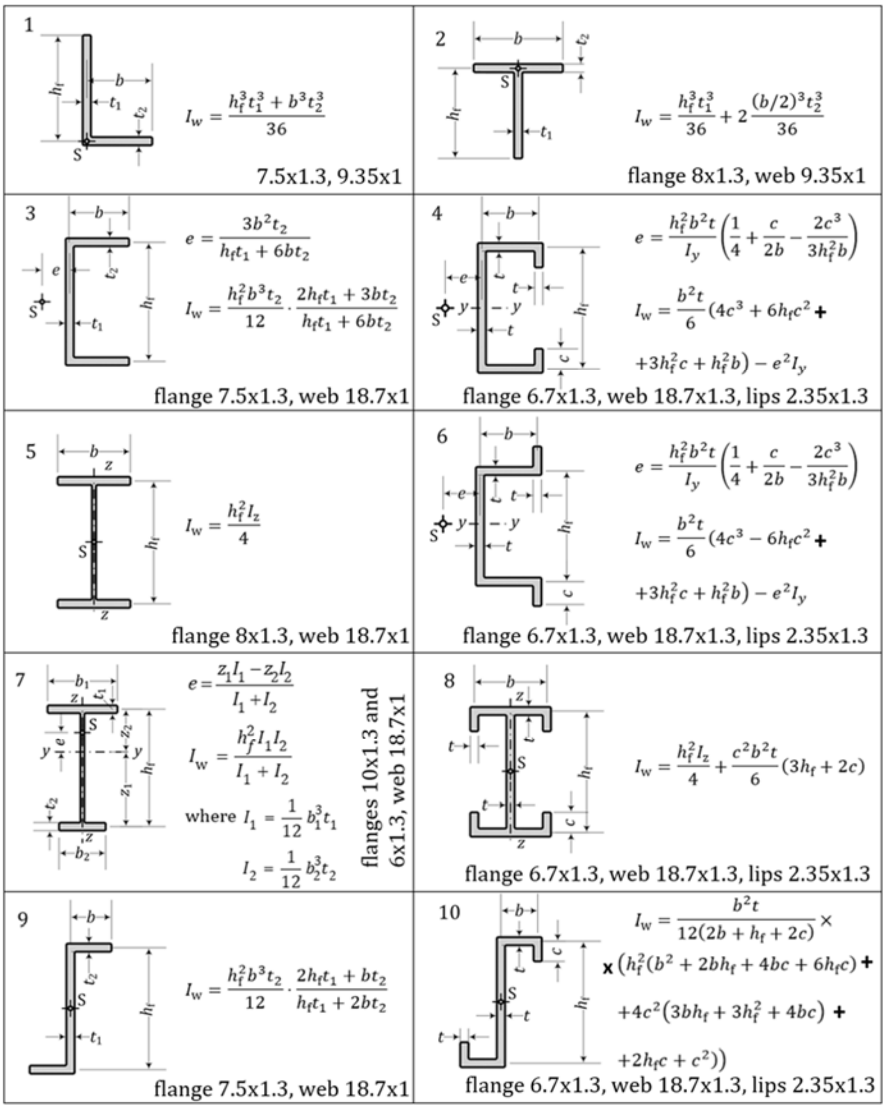

Table 6. Diamond cross-section dimensions (Figure 3c).

	Nodes, coordinates y = 0, z [mm], thicknesses t [mm]											
	0	1	2	3	4	5	6	7	8	9	10	11
z	0	20	50	70	90	90.86	100	120	140	170	190	200
t		10	10	17	17	140	140	17	17	10	10	110

Table 7. Oblique cross-section dimensions (Figure 7a).

	Nodes, coordinates y, z [mm], t = 0.4 [mm]						
	0	1	2	3	4	5	6
y	3.775	20	70	66.225	50	0	3.775
z	6.538	34.64	34.64	28.102	0	0	6.538

Table 8. Irregular cross-section dimensions (Figure 7b).

	Nodes, coordinates y, z [mm], thicknesses t [mm]										
	0	1	2	3	4	5	6	7	8	9	10
y	1.45	1.45	1.45	1.45	1.45	1.45	24.15	24.15	27.9	48.9	51.1

z	21.784	23.784	24.3	31.3	40.2	32.75	32.75	44.75	44.75	34.7	34.5
t	2.9	2.9	2.9	2.9	0	1.5	1.5	1.7	1.5	1.5	

	Nodes, coordinates y, z [mm], thicknesses t [mm]									
	10	11	12	13	14	15	16	17	18	19
y	51.1	56.7	59.3	63.55	63.55	63.55	63.55	63.55	1.45	1.45
z	34.5	37.5	37.5	34.6	18.043	16.3	7.3	0.85	0.85	21.784
t	1.5	1.5	1.6	2.9	2.9	3.3	2.9	1.7	2.9	

Table 9. Sigma cross-section dimensions (Figure 7c).

	Nodes, coordinates y, z [mm], t = 1.4 [mm]										
	0	1	2	3	4	5	6	7	8	9	10
y	60	55	0	0	10	10	10	0	0	60	65
z	30	0	0	40	50	100	150	160	200	200	170

The cross-section properties of the non-standard sections (diamond, oblique and irregular) and the sigma section appear in Table 10. They were verified by two calculation ways (see Key in Table 10).

Table 10. Cross-section properties of the a) diamond, b) oblique, c) irregular and d) sigma sections.

Quantity	Diamond section		Oblique section		Irregular section		Sigma section	
	Figure 3b	Figure 3c	Figure 7a		Figure 7b		Figure 7c	
	AA	TH	AA	TH	AA	TH	AA	TH
A cm^2	49.07	48.6	0.72	0.72	4.395	4.395	5.378	5.38
I_y cm^4	1492.56	1467	1.5199	1.5199	9.979	9.979	319.926	319.926
I_z cm^4	958.56	*	3.3399	3.3399	27.487	27.487	26.17	26.17
I_{yz} cm^4	0	0	0.8775	0.8775	-0.915	-0.916	4.358	4.358
α rad	0	0	0.384	0.384	-0.052	-0.0521	-0.015	-0.015
I_u cm^4	1492.56	1467	3.694	3.694	27.534	27.534	319.991	319.991
I_v cm^4	958.56	*	1.166	1.166	9.931	9.931	26.105	26.105
I_B cm^4	154.64	154.64 *	2.666	2.666	17.889	17.482	0.0351	0.0351
I_ω cm^6	9808.2	*	0.5556	-	15.545	-	2953.8	2953.84

Preprints.org (www.preprints.org) | NOT PEER-REVIEWED | Posted: 6 September 2024 doi:10.20944/preprints202409.0512.v1

y_G cm	0	0	3.5	3.5	3.1478	3.1478	2.1097	2.1097
z_G cm	11.849	11.763	1.732	1.732	1.9558	1.9558	10.13	10.13
y_S cm	0	0	3.5	-	3.3774	-	-1.77	-1.77
z_S cm	10.657	*	1.732	-	1.4318	-	10.99	10.99
$W_{pl,y}$ cm^3	219.24	214.746	0.868	0.863	6.051	6.0147	37.298	37.97

Key:

AA means that programmes (see chapter 3 Basis of Theory) were used by Antonio Agüero to calculate values;

TH means that the MathCad software was used by Torsten Höglund. See the example in Appendix 1;

* The Equivalent "compressed" model in Figure 3c cannot be used for the calculations of z-axis values;

I_B (Bredt torsion constant) relates to close sections (oblique and irregular sections), the closed part of a section (diamond section). For the sigma section, it is I_t (Saint Venant torsion constant);

NOTE: if all the section dimensions are increased n-times, the values of all the quantities will increase n^k-times depending on the quantity unit, where k = 1, 2, 3, 4, 6.

Table 10 shows a good agreement between the results of two ways of calculating cross-sections for **the** non-standard sections (diamond, oblique, irregular) and the sigma section. The values of the plastic section moduli for the 10 sections from Table 5 (No. 1 – No.1 0) and for four other sections (No.11 diamond, No.12 oblique, No.13 irregular, No.14 sigma section) are found in Table 11. There are three groups of plastic section moduli:

a) $W_{pl,y,nB}$, [$W_{pl,y}$], ($W_{pl,y}$), $W_{pl,z,nB}$ (see columns I.a, I.b, I.c, II.) is the bimoment is not (index nB) considered a constraint. The values in brackets [ ], ( ) in columns I.b and I.c are respectively calculated using the formula (G.39) in Annexe G, EN 1999-1-1:2023 [67], where it is formula (1). The MathCad software was employed for calculating the values in brackets. The corner details in column I.b for calculating [..]-values are (a)+(d) according to Figure 4. The corner details in column I.c for calculating (..)-values are (b)+(c) according to Figure 4. See the consequences described before Figure 4,

b) $W_{pl,y}$, $W_{pl,z}$, $W_{pl,w}$ (see columns III., IV., V.) when the bimoment is considered a constraint.

c) $W_{pl,y,max}$, $W_{pl,z,max}$, $W_{pl,w,max}$ (see columns VI., VII., VIII). These values may be obtained only if the given internal force exists with some other concominant internal force. See Tables 15a,b for the monosymmetric I-shaped section, Tables 16a,b for the channel section and Tables 17a,b for the Z-section.

All the W_{pl} values in Table 11, except the "MathCad values" in columns I.b and I.c, were calculated using the computer programmes described in Chapter 3: Basis of Theory. The model with overlapping in corners (a+d) according to Figure 4 is taken into account in Chapter 3: Basis of Theory. Other exceptions are: 1) the values in italics for the channel (No.3) and the Z-section (No.9), which were calculated using the formulae designated for practice, and appear in Table 16a for the channel and in Table 17a for the Z-section; 2) the values with an asterisk (*) in boxes 9-VI (row No.-column No.) and 10-VI were also calculated using the MathCad formulae; 3) only the value in box 11-I.b was calculated for the compressed equivalent shape of the cross-section given in Figure 3c. All the other values for the diamond section (No.11) were calculated for the real cross-section shape in Figure 3b.

The values in **bold** in boxes 9-VI, 10-VI and 12-VI are the resistances that can be reached for continuously laterally supported sections. The concomitant bimoment for the Z-section is zero (see Table 17a).

A special case is Z-section, for which more results are provided in Table 12.

Table 11. Values of the various kinds of plastic section moduli: $W_{pl,y}$ and $W_{pl,z}$ [cm^3], $W_{pl,w}$ [cm^4].

 doi:10.20944/preprints202409.0512.v1

Section		I.a	I.b	I.c	II.	III.	IV.	V.	VI.	VII.	VIII.
		The bimoment is not considered a constraint				The bimoment is considered a constraint			$W_{pl,max}$		
No.	Shape	$W_{pl,y,nB}$	[$W_{pl,y}$]	($W_{pl,y}$)	$W_{pl,z,nB}$	$W_{pl,y}$	$W_{pl,z}$	$W_{pl,w}$	$W_{pl,y,max}$	$W_{pl,z,max}$	$W_{pl,w,max}$
1	L	27.77	–	–	43.15	–	–	–	37.47	55.16	–
2	T	44.81	44.81	44.51	23.14	–	–	–	51.209	23.14	–
3	U	269.7 –	269.7 –	– –	74.14 –	241.4 *240.6*	74.14 *73.06*	592.6 *591.1*	269.7 *269.7*	81.31 *81.12*	631.7 *610.3*
4	U + lips inside	326.5	326.5	–	100.96	300.6	100.96	879.8	326.5	113.4	914.9
5	I doub. symm.	281.9	281.9	270.2	46.2	281.9	46.2	388.9	281.9	46.2	388.9
6	U + lips outside	340.8	340.8	–	100.9	298	100.9	758.7	340.8	113.4	769.3
7	I mono symm.	279.4	275.1	263.4	48.87	279.4	44.19	234.3	281.8	48.87	287.9
8	I + lips doub.s	376.4	376.4	361.2	78.	376.4	78.	703.	376.4	78.	703.
9	Z point symm.	166.4 – –	– – –	– – –	64.70 – –	166.4 *162.9* –	64.70 *63.22* –	683 *687.5* –	**269.7** **269.7** **269.7***	77.8 *73.13* –	760. *758.5* –
10	Z + lips point s.	205.8	–	–	90.9	205.8	90.9	976.5	**326.4** **326.5***	107.4	1123.
11	Sect. + diamon	219.9	214.7	–	160.	219.9	147.	307	230.	160.	415.
12	Oblique point s.	0.866	0.863	–	1.301	0.866	1.301	0.173	**0.97**	1.4	0.173
13	Irregu-lar sec.	6.05	6.014	–	9.954	5.955	9.933	7.022	6.09	10.05	7.227
14	Sigma asymm	37.30	37.97	–	9.036	34.9	8.96	95.9	38.	10.5	104.

Key: Index w – warping

The way how to obtain W_{pl} values and, consequently, interaction diagrams is explained in Chapter 3, where the used software is described.

The following are facts (see Table 11):

a) for the doubly symmetric sections (No. 5, 8):

$W_{pl,y} = W_{pl,y,nB} = W_{pl,y,max}$; $W_{pl,z} = W_{pl,z,nB} = W_{pl,z,max}$; $W_{pl,w} = W_{pl,w,max}$;

b) for the monosymmetric sections with axis of symmetry z (No. 2, 7, 11):

$W_{pl,y} = W_{pl,y,nB} < W_{pl,y,max}$; $W_{pl,z} < W_{pl,z,nB} = W_{pl,z,max}$; $W_{pl,w} < W_{pl,w,max}$;

c) for the monosymmetric sections with axis of symmetry y (No. 3, 4, 6):

$W_{pl,y} < W_{pl,y,nB} = W_{pl,y,max}$; $W_{pl,z} = W_{pl,z,nB} < W_{pl,z,max}$; $W_{pl,w} < W_{pl,w,max}$;

d) for the point symmetric sections (9, 10):

$W_{pl,y} = W_{pl,y,nB} < W_{pl,y,max}$; $W_{pl,z} = W_{pl,z,nB} < W_{pl,z,max}$; $W_{pl,w} < W_{pl,w,max}$;

e) asymmetric sections are: No. 1, 12, 13, 14;

f) for non-warping cross-sections or for cross-sections with negligible warping through element thicknesses, the calculation of $W_{pl,y}$, $W_{pl,z}$, $W_{pl,w}$ for bimoment $B_{Ed,}$ considered a constraint, is not

Preprints.org (www.preprints.org) | NOT PEER-REVIEWED | Posted: 6 September 2024 doi:10.20944/preprints202409.0512.v1

possible. See sections No. 1 and 2, columns III. – V.

For the Z-section, more W_{pl} values for are found in Table 12. The W_{pl} values are given for both axes *yz*, and also for the principal axes *uv* (see Figure 8 for the Z-section with lips). Abbreviation "ST" indicates that values are obtained by calculation with the help of the DLUBALs programme's SHAPE THIN for the model with *b* details of corners, but with no element with zero thickness (Figure 4b). "Dt" means that values are taken from database of the DLUBALs programme's SHAPE THIN.

Table 12. Comparisons of various W_{pl} values of the plastic section modulus for the Z-section without lips: $W_{pl,y}$ and $W_{pl,z}$ [cm^3], $W_{pl,w}$ [cm^4].

		I.a	I.b	I.c	II.	III.	IV.	V.	VI.	VII.	VIII.
Section		The bimoment not considered a constraint				The bimoment considered a constraint			$W_{pl,max}$		
No.	Shape, axes *yz*	$W_{pl,y,nB}$	–	–	$W_{pl,z,nB}$	$W_{pl,y}$	$W_{pl,z}$	$W_{pl,w}$	$W_{pl,y.max}$	$W_{pl,z.max}$	$W_{pl,w.max}$
9 *yz*	Z point symm.	166.4	–	–	64.70	166.4	64.70	683.	**269.7**	77.8	760.
		–	–	–	–	*162.9*	*63.22*	*687.5*	**269.7**	*73.13*	*758.5*
		–	–	–	–	–	–	–	**270.2 ST**	77.8 **ST**	–
		–	–	–	–	151.2	60.6	671	**274.8 Dt**	77.0 **Dt**	–
		–	–	–	–	–	–	–	**269.7***	–	–
N	Shape, axes *u,v*	$W_{pl,unB}$	–	–	$W_{pl,vnB}$	$W_{pl,u}$	$W_{pl,v}$	$W_{pl,w}$	$W_{pl,u.max}$	$W_{pl,v.max}$	$W_{pl,w.max}$
9 *uv*	Z point symm.	246.7	–	–	63.73	–	–	683	279.51	66.19	760.
		–	–	–	63.68 ST	–	–	–	279.5 ST	63.68 ST	–
		239. Dt	–	–	62.1 Dt	–	–	–	283.8 Dt	63.95 Dt	–

The W_{pl} values of the plastic section modulus of the cross-sections with various shapes were calculated in several ways and by various computer programmes. All the comparisons show excellent and acceptable agreements. The correctness of values is proved.

The results of programmes https://laboratoriosvirtuales.upv.es/webapps/thinwallsectiongeneral.html and https://labmatlab-was.upv.es/webapps/home/thinwallsectionopenclosed.html are presented in Figures 9 – 13, 16, 18, 24 and 26. Figures 9a,b – 13a,b, 16a,b and 18a,b present interaction diagrams for the given cross-sections with a combination of internal forces N_{Ed}, $M_{y,Ed}$, $M_{z,Ed}$ for both cases: a) without considering bimoment B_{Ed} to be a constraint, b) with bimoment $B_{Ed} = 0$ kNm^2 considered a constraint. Interaction diagrams can be used for any values N_{Ed}, $M_{y,Ed}$, $M_{z,Ed}$ because diagrams are accompanied by relevant A and W_{pl} values. Figures 24a,b and 26 show the interaction diagrams for the combination of internal forces $M_{y,Ed}$, $M_{z,Ed}$, B_{Ed}. In all the interaction diagrams, the following sign convention of internal forces is accepted: tension axial force N_{Ed} is positive; bending moment $M_{y,Ed}$ is positive when the bottom cross-section part is in tension and the upper part in compression; bending moment $M_{z,Ed}$ is positive when the right-hand cross-section part is in tension and the left-hand part in compression. The sign convention of bimoment B_{Ed} is clear from Figures 21 and 22. In the cross-section resistances, calculation safety factor $\gamma_{M0} = 1.0$ is used for steel profiles because it is prescribed in [65], and $\gamma_{M1} = 1.1$ is employed for aluminium profiles [67].

Preprints.org (www.preprints.org) | NOT PEER-REVIEWED | Posted: 6 September 2024 doi:10.20944/preprints202409.0512.v1

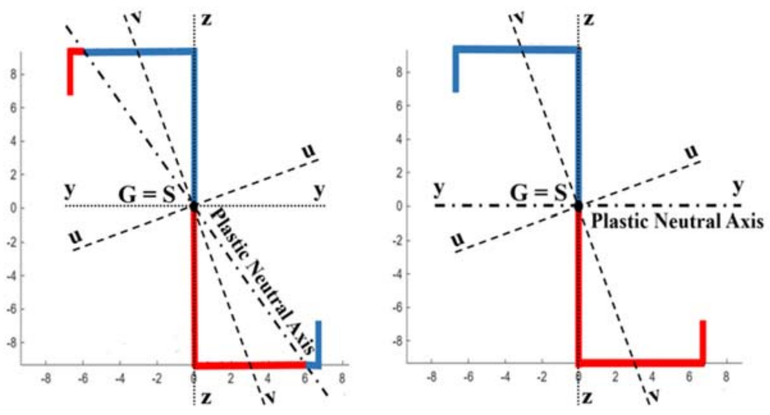

a) **b)**

Figure 8. The Z-section with lips (no. 10 in Tables 5 and 11) under bending moment $M_{y,\mathrm{Ed}}$ about axis y-y with axes yz and principal axes uv. a) The location of the plastic neutral axis (PNA) responds to stress distribution to obtain $M_{\mathrm{pl,y}}$. In this case, the results are the same regardless of bimoment constraint being considered or not. b) The location of the PNA responds to the stress distribution to obtain $M_{\mathrm{pl,y,max}}$. When the beam is loaded in the z-direction and is continuously and laterally supported in the y-direction, concomitant $M_{\mathrm{z,conc}}$ may appear.

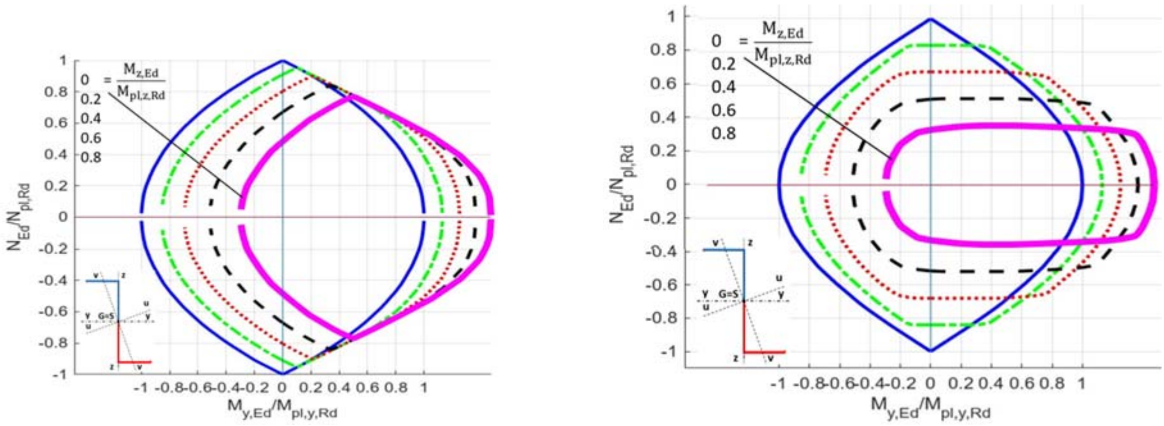

a) **b)**

Figure 9. The Z-section without lips (no. 9 in Tables 5 and 11) with A = 38.2 cm^2. See Table 11. The interaction diagrams for the cross-section under combination $N_{\mathrm{Ed}} + M_{y,\mathrm{Ed}} + M_{z,\ \mathrm{Ed}}$ calculated: a) without considering bimoment B_{Ed} a constraint: $W_{\mathrm{pl,y,nB}}$ = 166.4 cm^3, $W_{\mathrm{pl,z,nB}}$ = 64.7 cm^3; b) with bimoment B_{Ed} = 0 considering kNm^2 a constraint: $W_{\mathrm{pl,y}}$ = 166.4 cm^3, $W_{\mathrm{pl,z}}$ = 64.7 cm^3.

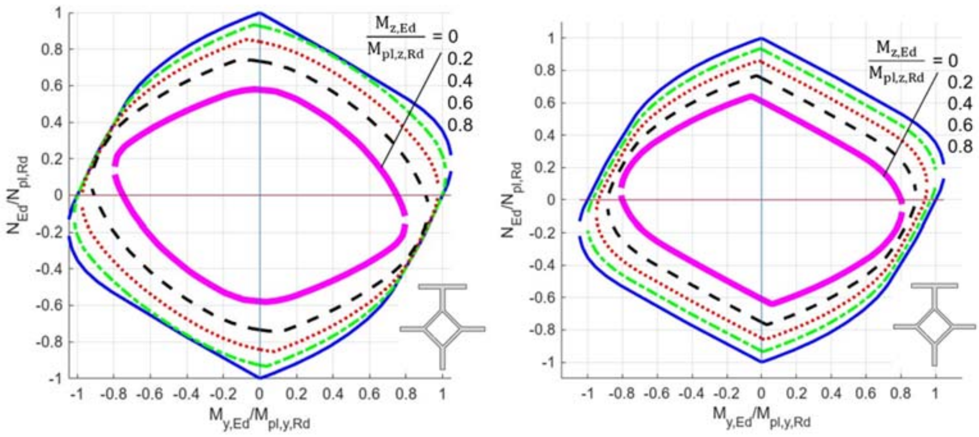

a) **b)**

Figure 10. The diamond section (no. 11 in Tables 5 and 11) with A = 49.07 cm^2. See Table 11. The interaction diagrams for the cross-section under combination $N_{\mathrm{Ed}} + M_{y,\mathrm{Ed}} + M_{z,\mathrm{Ed}}$ calculated: a) without considering bimoment B_{Ed} a constraint: $W_{\mathrm{pl},y,\mathrm{nB}}$ = 219.9 cm^3, $W_{\mathrm{pl},z,\mathrm{nB}}$ = 160 cm^3; b) with bimoment B_{Ed} = 0 kNm^2 considered a constraint: $W_{\mathrm{pl},y}$ = 219.9 cm^3, $W_{\mathrm{pl},z}$ = 147 cm$^{3.}$

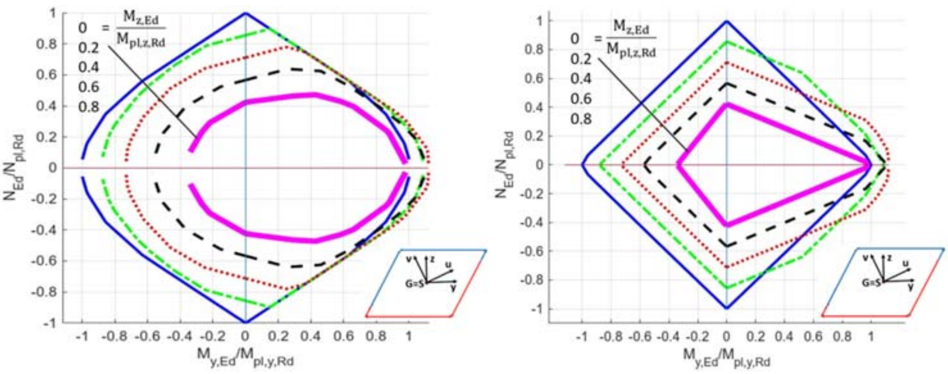

a) **b)**

Figure 11. The oblique section (no. 12 in Tables 5 and 11) with A = 0.72cm^2. See Table 11. The interaction diagrams for the cross-section under combination $N_{\mathrm{Ed}} + M_{y,\mathrm{Ed}} + M_{z,\mathrm{Ed}}$ calculated: a) without considering bimoment B_{Ed} a constraint: $W_{\mathrm{pl},y,\mathrm{nB}}$ = 0.866 cm^3, $W_{\mathrm{pl},z,\mathrm{nB}}$ = 1.301 cm^3;b) with bimoment B_{Ed} = 0 kNm^2 considered a constraint: $W_{\mathrm{pl},y}$ = 0.866 cm^3, $W_{\mathrm{pl},z}$ = 1.301 cm$^{3.}$

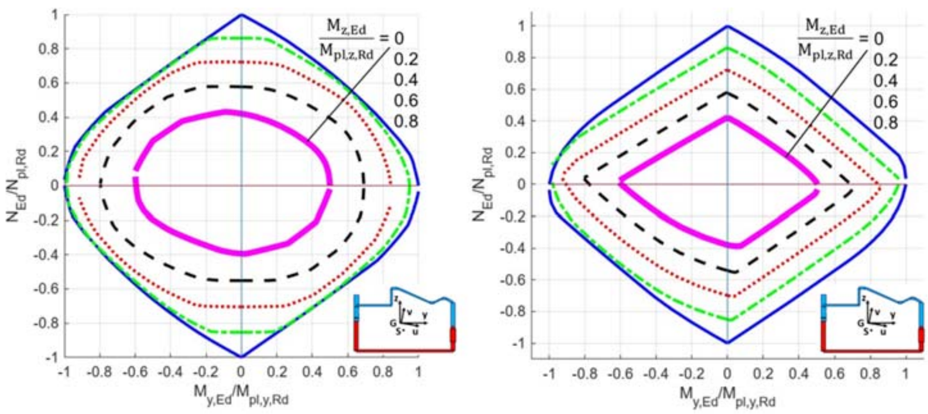

a) **b)**

Figure 1. The Irregular section (no. 13 in Tables 5 and 11) with A = 4.395 cm^2. See Table 11. The interaction diagrams for the cross-section under combination $N_{\mathrm{Ed}} + M_{y,\mathrm{Ed}} + M_{z,\mathrm{Ed}}$ calculated: a) without considering bimoment B_{Ed} a constraint: $W_{\mathrm{pl},y,\mathrm{nB}}$ = 6.05 cm^3, $W_{\mathrm{pl},z,\mathrm{nB}}$ = 9.954 cm^3; b) with bimoment B_{Ed} = 0 kNm^2 considered a constraint: $W_{\mathrm{pl},y}$ = 5.955 cm^3, W_{plz} = 9.933 cm$^{3.}$

 doi:10.20944/preprints202409.0512.v1

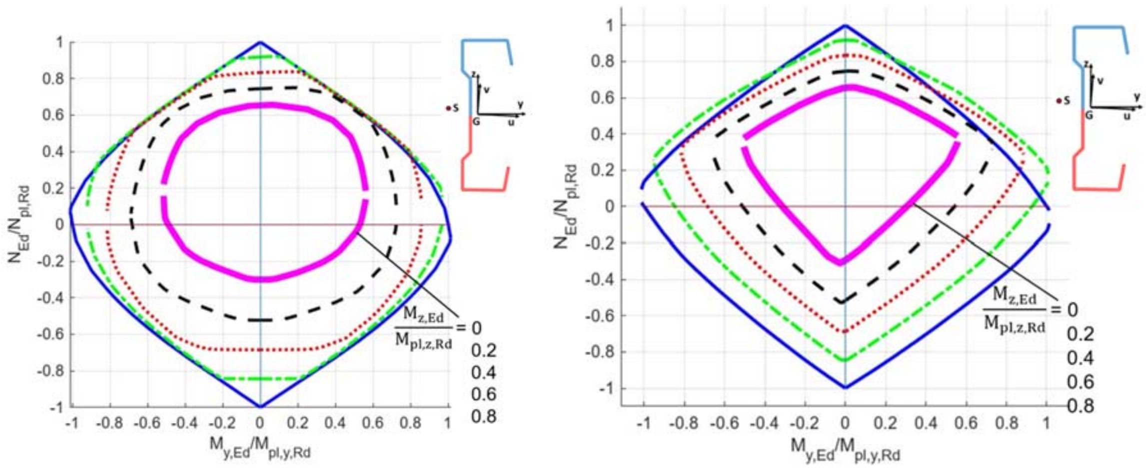

a) **b)**

Figure 13. The sigma section (no. 14 in Tables 5 and 11) with A = 5.378 cm². See Table 11. The interaction diagrams for the cross-section undercombination $N_{Ed} + M_{y,Ed} + M_{z,Ed}$ calculated: a) without considering bimoment B_{Ed} a constraint: $W_{pl,y,nB}$ = 37.3 cm³, $W_{pl,z,nB}$ = 9.036 cm³; b) with bimoment B_{Ed} = 0 kNm² considered a constraint: $W_{pl,y}$ = 34.9 cm³, $W_{pl,z}$ = 8.96 cm³.

5. Recommendations

The computer programmes in Chapter 3: Basis of Theory enable the plastic reserve of the cross-sections with any shape and under any combination of eight internal forces to be investigated. Below recommendations for the frequent special partial cases are offered.

5.1. Double Symmetric Steel I-Shaped Cross-Section of Class 1 or Class 2 under the Combination of Axial Force and Bending Moment $N_{Ed} + M_{y,Ed}$.

Baláž [64] solved the problems in 8.2.9.1 [65] as follows. Using the approximate formulas (8.43) and (8.48) in [65] leads to two problems:
a) the approximate formula (8.48) after substitution into the formula (8.43) in the form of:

$$\frac{M_{y,Ed}}{M_{N,y,Rd}} = \frac{M_{y,Ed}}{M_{pl,y,Rd}}\frac{1-0.5a}{1-n} = m_y\frac{1-0.5a}{1-n} \leq 1.0 \quad \text{but} \quad m_y = \frac{M_{y,Ed}}{M_{pl,y,Rd}} \leq 1.0\ ,\ n = \frac{N_{Ed}}{N_{pl,Rd}} \tag{27}$$

Formula (27) confers both numerical instability and the looping of the automated calculation high relative axial force n (if n approaches the 1.0 value) values when designing cross-section size. For the selected cross-sectional size, verification may have a high utilisation value (e. g. more than 3.0). When increasing the cross-section size by one step, verification of utilisation can show a big uneconomical design, and so on. It leads to never ending looping. The solution is to modify EN formulae (27) before programming in form (28), in which there is no division by expression (1-n) which, for n approaching 1.0, leads to division by a number approaching zero.

$$\max[n + (1-0.5a)m_y; m_y] \leq 1.0\ ,\quad n = \frac{N_{Ed}}{N_{pl,Rd}}\ ,\quad m_y = \frac{M_{y,Ed}}{M_{pl,y,Rd}}\ ,\quad a = \min[(A - 2bt_f)/A; 0.5] \tag{28}$$

Numerical example:

HEA 300, S355, f_y = 355 MPa, γ_{M0} = 1.0, N_{Ed} = 3795 kN, n = 0.95, $M_{y,Ed}$ = 100 kNm, m_y = 0.204.

Formula (27) [65] gives utilisation factor U_{EN} = 3.574, but requires a much bigger HEA size. According to the proposed formula (28), the correct utilisation factor is only U = 1.128. If the bigger HEA 340 size is chosen, formula (27) gives U_{EN} = 0.665, which indicates a big uneconomical design, but the real utilisation factor is U = 0.933 according to (28). Employing EN formula (27) leads to never ending looping.

In the same way, it is necessary to rearrange formulae (8.49), (8.50) and (8.43) in [65] to avoid numerical instability for the I-shaped cross-sections under axial force N_{Ed} and at bending moment

Preprints.org (www.preprints.org) | NOT PEER-REVIEWED | Posted: 6 September 2024 doi:10.20944/preprints202409.0512.v1

$M_{z,Ed}$. Baláž proposed [64] using instead EN 1993-1-1 [65] formulae (8.49), (8.50) and (8.43): $(\boldsymbol{n}-\boldsymbol{a})^2+\boldsymbol{a}(2-\boldsymbol{a})+(1-\boldsymbol{a})^2\boldsymbol{m_z}\le 1.0$, if $\boldsymbol{n}>\boldsymbol{a}$, $\boldsymbol{n}=\frac{N_{Ed}}{N_{pl,Rd}}$, $\boldsymbol{m_z}=\frac{M_{z,Ed}}{M_{pl,z,Rd}}$ (29)

$\boldsymbol{m_z}\le 1.0$, if $\boldsymbol{n}\le\boldsymbol{a}$, $\boldsymbol{a}=\min[(A-2bt_f)/A;0.5]$ (30)

Formulae (8.51), (8.52) and (8.43) in [59] are valid for rectangular hollow sections, and must also be rearranged before programming in the same way as formulae (8.48) and (8.43); see Eq. (28), to avoid dividing by a value that approaches zero if relative axial force n approaches 1.0.

b) Formula (27) provides results on the dangerous side for low axial force values (error goes up to approximately 7%). This problem can be solved by replacing the approximate Eurocode formulae (8.43), (8.48) here (27) with the more accurate formulae derived by Baláž [64]. For I-shaped sections, we present the exact m_y-n interaction formulae in two versions:

b1) for a cross-section consisting of three rectangles, two independent dimensionless parameters appear in formulae. The graphic interpretation is found in Figures 14 and 15. Formula (31) is valid for low $\boldsymbol{n}<\boldsymbol{a}$ values when the PNA lies in the web of the I-section (see the bottom left-hand part of Figure 15). Formula (32) is valid for higher s $\boldsymbol{n}>\boldsymbol{a}$ values when the PNA lies on the I-section flange (see the bottom right-hand part of Figure 14). If $\boldsymbol{n}=\boldsymbol{a}$, the PNA is located at the point of contact of the flange with the web.

$$m_y=1-\frac{n^2}{1-\left(\frac{A_w}{A}-1\right)^2\left(1-\frac{t_w}{b}\right)}, \quad \text{if} \quad n\le a=\frac{1-2bt_f}{A}=\frac{A_w}{A}\approx\frac{h_wt_w}{h_wt_w+2bt_f}, \quad h_w=h-2t_f$$

(31)

$$m_y=1-\frac{n^2-\left(\frac{A_w}{A}-n\right)^2\left(1-\frac{t_w}{b}\right)}{1-\left(\frac{A_w}{A}-1\right)^2\left(1-\frac{t_w}{b}\right)}, \text{if} \quad n\ge a=\frac{1-2bt_w}{A}=\frac{A_w}{A}\approx\frac{h_wt_w}{h_wt_w+2bt_f} \qquad (32)$$

b2) for the cross-section consisting of a midline with thicknesses, only one independent dimensionless parameter appears in the formulae.

$$m_y=1-\frac{n^2}{1-\left(\frac{A_{w.st}}{A_{st}}-1\right)^2}, \text{if} \quad n\le\frac{A_{w.st}}{A_{st}}=\frac{h_ft_w}{h_ft_w+2bt_f}, \quad h_f=h-t_f \qquad (33)$$

$$m_y=\frac{1-n}{1-0{,}5\frac{A_{w.st}}{A_{st}}}, \text{if} \quad n\ge\frac{A_{w.st}}{A_{st}}=\frac{h_ft_w}{h_ft_w+2bt_f} \qquad (34)$$

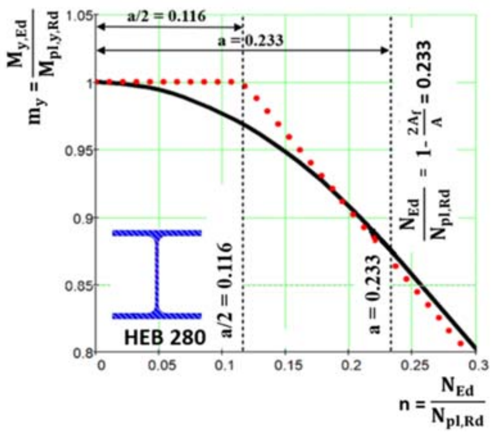

 doi:10.20944/preprints202409.0512.v1

Figure 14. Detail of Figure 15.

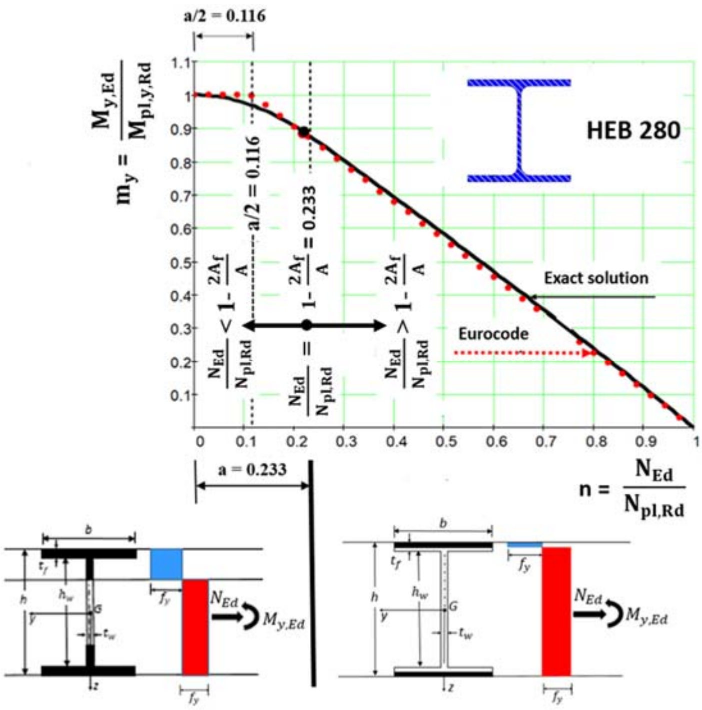

Figure 15. Geometrical interpretations of interaction $m_y - n$ formulae for the HEB 280 section under the combination of axial force N_{Ed} and moment $M_{y,Ed}$. Comparison of: a) the approximate red dotted bilinear function defined in EN 1993-1-1 [65] by formula (27) or (28) with b) a black solid line representing the non-linear function defined by exact formulae (31) and (32) [64].

For n = a/2, the approximate solution gives the value with a ≤ 7% error on the dangerous side. The axial force effect can be neglected if $n \leq \min\,(0.25; 0.5 h_w t_w / A\,)$, which is approximately $n \leq \min\,(0.25; a/2\,)$ with $a = \min\left[\left(A - 2bt_f\right)/A; 0.5\right]$. S235 f_y =235 MPa, safety factor γ_{M0} = 1.0. For an exact cross-section shape: $N_{pl,Rd}$ = 3 087 kN, $M_{pl,y,Rd}$ = 360.6 kNm, $M_{pl,z,Rd}$ = 168.6 kNm. For the midline model: $N_{pl,Rd}$ = 3 015.3 kN, $M_{pl,y,Rd}$ = 352.66 kNm, $M_{pl,z,Rd}$ = 165.82 kNm.

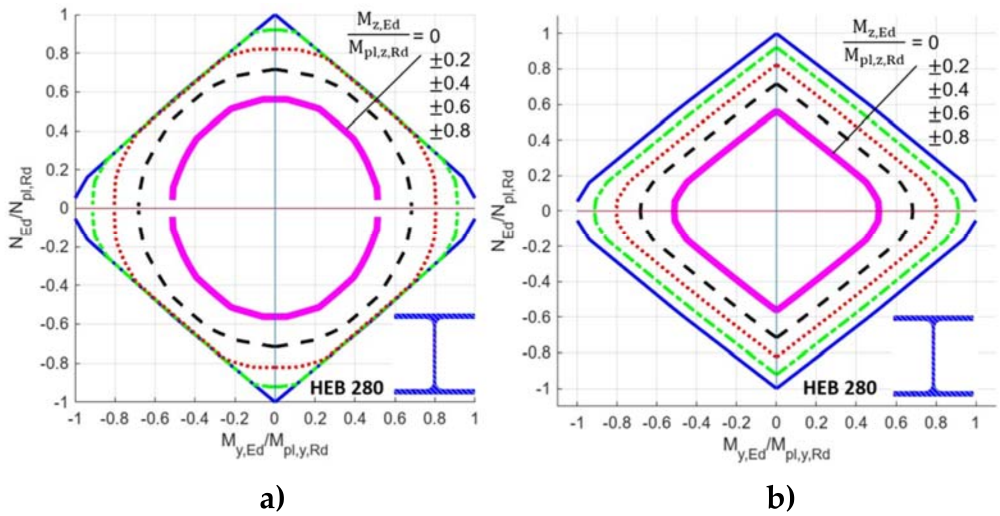

Figure 16. The HEB 280 section with A = 128.31 cm², $W_{pl,y}$ = 1 500.67 cm³, $W_{pl,z}$ = 705.6 cm³, $W_{pl,w}$ = 9 243.36 cm⁴ for the midline model. The interaction diagrams for the cross-section under combination N_{Ed} + $M_{y,Ed}$ + $M_{z,Ed}$ calculated: a) without considering bimoment B_{Ed} a constraint ; b) with bimoment B_{Ed} = 0 kNm² considered a constraint.

5.2. Plastic Reserve of the Steel Channel Cross-Section under Bending Moment $M_{y,Ed}$

Preprints.org (www.preprints.org) | NOT PEER-REVIEWED | Posted: 6 September 2024 doi:10.20944/preprints202409.0512.v1

The maximum positive plastic moment in channel $M_{pl,y,max} = W_{pl,y,max}\ f_y$ can be achieved only with negative concomitant bimoment $B_{Ed,conc}$. As the continuously and laterally supported beam cannot rotate, bimoment $B = 0$ kNm^2 and $M_{pl,y,max}$ cannot be achieved. Only the value of the elastic-plastic moment $M_{pl,y} = W_{pl,y}\, f_y$ can be achieved. The values of plastic reserves (shape factors) for I-sections, channel and similar sections are very low. For UPE 360, shape factors are: $\alpha_{pl,y} =$ 875.3/823.6 = 1.063, $\alpha_{pl,y,max} =$ 982.6/823.6=1.193. For sections of this type under single bending moment $M_{y,Ed}$, the utility of the plastic reserve is negligible.

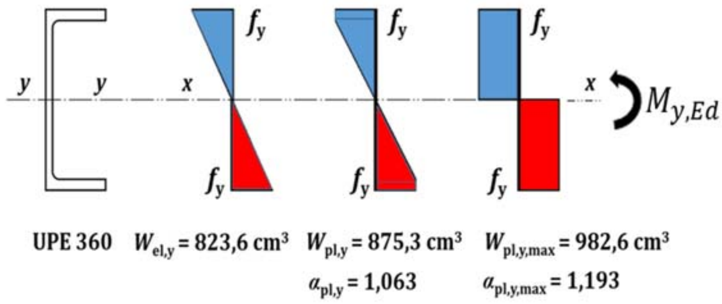

Figure 17. The plastic reserves (shape factors $\alpha_{pl,y}$ and $\alpha_{pl,y,max}$) of the UPE 360 profile [60]. Above W_{pl}-, values are calculated for the exact cross-section shape. In paragraph 5.4, W_{pl}-values are calculated for the midline model: $A = 76.52$ cm^2, $W_{el,y} = W_{pl,y} = 841.7$ cm^3, $W_{pl,y,max} = 959.37$ cm^3.

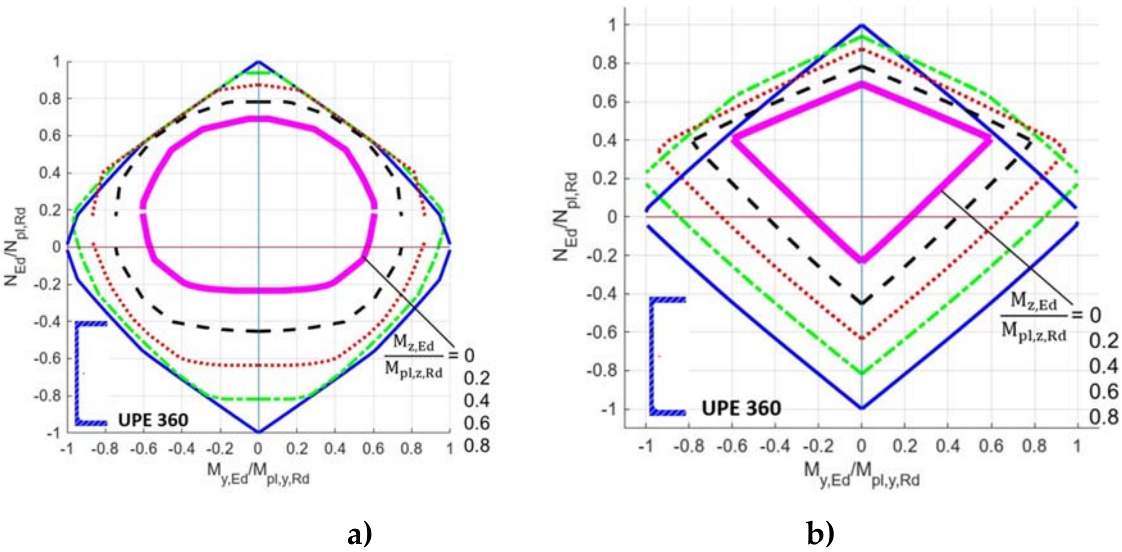

Figure 18. The UPE 360 section. S235, f_y =235 MPa, safety factor $\gamma_{M0} = 1.0$. For the midline model: $N_{pl,Rd}$ = 1798 kN, $M_{pl,z,Rd}$ = 44.24 kNm. Interaction diagrams $N_{Ed} + M_{y,Ed} + M_{z,Ed}$ are calculated: a) without considering bimoment B_{Ed} a constraint $M_{pl,y,Rd}$ = 225.45 kNm. 225.452 kNm in Table 14; b) with bimoment $B_{Ed} = 0$ kNm^2 considered a constraint: $M_{pl,y,Rd}$ = 197.80 kNm. 199.52 kNm in Table 14.

5.3. Double Symmetric Aluminium and Steel I-Shaped Profiles under the Combination of Bending Moment about y-y Axis and Bimoment $M_{y,Ed} + B_{Ed}$

The metal (steel and aluminium) Eurocodes give plastic cross-section interaction formulae that lead to a more economic design. Formulae are valid for I-shaped sections and others. Almost nothing relates to the interaction with torsional bimoment. Nothing is provided for channels, which are frequently used in practice. The steel Eurocode does not allow the use of plastic resistance, which takes strengthening into account. However, the aluminium Eurocode enables ultimate axial load N_u and ultimate bending moment M_u to be calculated in the collapse limit state from the formulae in Annexes F.4 and F.5 in [67].

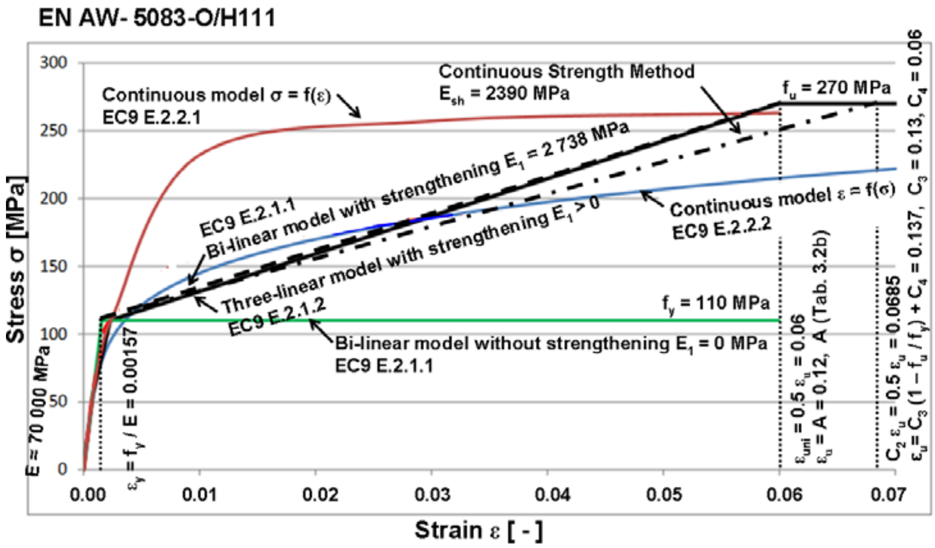

Figure 19. Comparisons of the five stress-strain relations given in [68] with the Continuous Strength. Method (CSM) [70] applied in [71] for non-heat treatable wrought aluminium alloy EN AW-5083-O/H111. The continuous model incorrectly defined in E.2.2.1 [68] was later corrected thanks to the findings in [72].

In 1958, Streľbickaja [53] theoretically and experimentally investigated I- and U-sections under any combinations of five internal forces: two bending internal forces $M_{y,Ed}$ and $V_{z,ed}$ and three torsional internal forces B_{Ed}, $T_{w,Ed}$ and $T_{t,Ed}$. For any of these combinations, the following resistances were defined and calculated: (i) elastic; (ii) plastic without strengthening; (iii) plastic with strengthening. Some of the analytical formulae given in [53] were verified by computer programmes in [73, 74]. Comparisons show the genius of Ukrainian lady Streľbickaja [53].

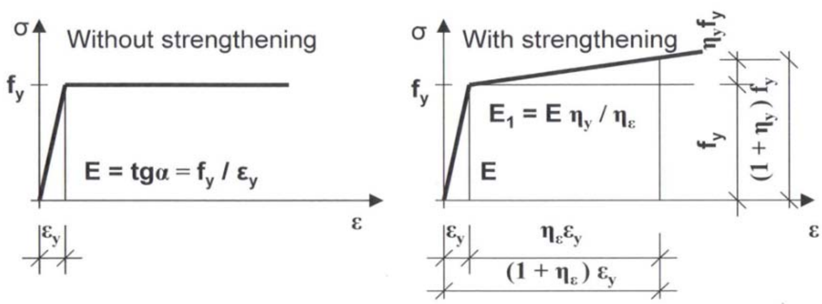

Figure 20. Bilinear stress-strain diagrams without and with strengthening. Definitions of η_ε and η_y [53].

Resistance calculation according to Streľbickaja [53]

$$W_{el,y} = t_f b_f h_f + t_w h_f^2 / 6 = 1.14 \text{ x } 10 \text{ x } 18.86 + 0.7 \text{ x } 18.86^2 / 6 = 256.502 \text{ cm}^3 \quad (35)$$

$$W_{pl,y} = t_f b_f h_f + t_w h_f^2 / 4 = 1.14 \text{ x } 10 \text{ x } 18.86 + 0.7 \text{ x } 18.86^2 / 4 = 277.251 \text{ cm}^3 \quad (36)$$

$$M_{el,y,Rd} = W_{y,el} f_y / \gamma_{M0} = 256502 \text{ x } 110 / 1.0 = 28.215 \text{ kNm} \quad (37)$$

$$M_{pl,y,Rd} = W_{y,pl} f_y / \gamma_{M0} = 277251 \text{ x } 110 / 1.0 = 30.498 \text{ kNm} \quad (38)$$

$$W_{el,w} = t_f h_f b_f^2/6 = 358.34\,\mathrm{cm}^4,\ B_{el,Rd} = W_{el,w} f_y/\gamma_{M0} = 0.394\,\mathrm{kNm}^2 \quad (39)$$

$$W_{pl,w} = t_f h_f b_f^2/6 = 537.51\,\mathrm{cm}^4,\ B_{pl,Rd} = W_{w,pl} f_y/\gamma_{M0} = 0.591\,\mathrm{kNm}^2 \quad (40)$$

For given distance u, the size of small elastic core 2e (Figure 21a) can be calculated from Eq. (41).

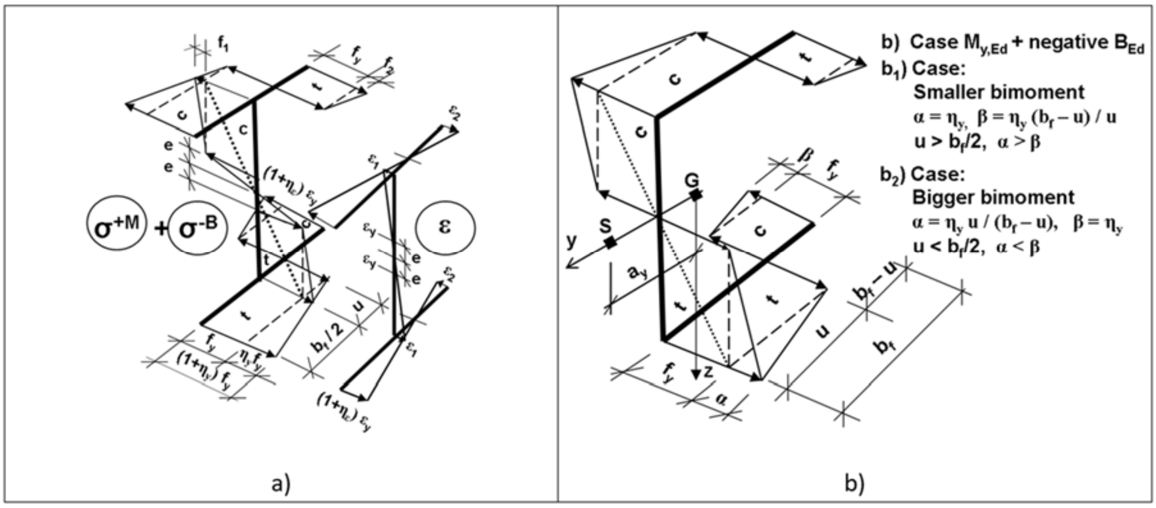

Figure 21. Normal stress distribution in: a) an I-shaped section (e = 0 mm is possible) and b) channel under the combination of positive bending moment $M_{y,Ed}$ and negative bimoment B_{Ed} (sign convention: see Figure 22):.

(i) elastic limit state defined by $\sigma_{max} = f_y$ – dotted line (c – compression, t – tension);
(ii) plastic limit state without strengthening defined by $\sigma_{max} = f_y$ – dashed line;
(iii) plastic limit state with strengthening defined by $\varepsilon_{max} = (1 + \eta\varepsilon)\varepsilon_y$ – solid line with related ε distribution.

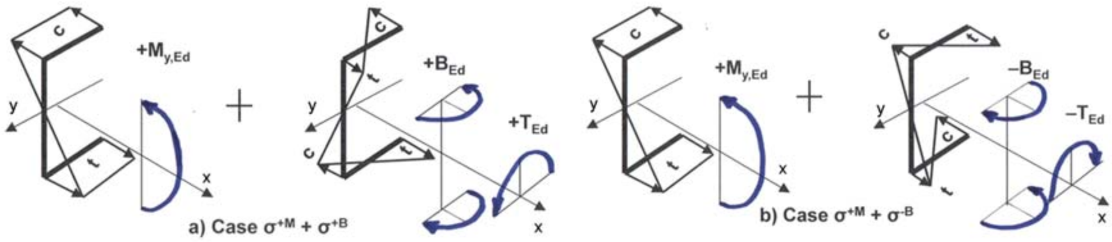

Figure 22. Sign convention. Combination of moment $M_{y,Ed}$ with: a) positive and b) negative bimoment B_{Ed}.

$$e(u) = \left(1 + \frac{b_f}{2u}\right)\frac{h_f}{2\eta_\varepsilon} \quad (41)$$

(i) The elastic limit state is defined by the linear interaction formula:

$$\frac{M_{y,Ed}}{M_{el,y,Rd}} + \frac{B_{Ed}}{B_{el,Rd}} \le 1.0 \quad (42)$$

From Figure 21a, plastic resistances may be derived as functions of distance u by defining the position of the neutral axis in the I-section under the bending moment $M_{y,Ed}$ and bimoment B_{Ed} interaction. For the plastic limit state:
(ii) without strengthening $\eta_y = 0$ (Figure 19, Figure 20):

 doi:10.20944/preprints202409.0512.v1

$$M_{y,Ed}(u)=\left[2t_f u h_f+\left(\frac{h_f^2}{4}-\frac{e(u)^2}{3}\right)t_w\right]f_y,\quad B_{Ed}(u)=\left(\frac{b_f^2}{4}-u^2\right)t_f h_f f_y \tag{43}$$

(iii) with strengthening η_y = 0.25 (Figure 19)

$$M_{y,Ed,s}(u)=M_{y,Ed}(u)+\left[t_f b_f h_f+\left(\frac{h_f^2}{6}-\frac{e(u)^2}{3}-\frac{h_f}{6}e(u)^2\right)t_w\right]\frac{u}{u+0.5b_f}\eta_y f_y \tag{44}$$

$$B_{Ed,s}(u)=B_{Ed}(u)+\frac{t_f b_f^3 h_f}{12\left(u+0.5b_f\right)}\eta_y f_y \tag{45}$$

The obtained numerical results [71] appear in Table 13. Without strengthening, the results are compared to the numerical results of the DUENQ computer programme [73], which uses the simplex method and the QST-TSV-3Blech computer programme [74] based on Kindmann`s and Frickel`s method called the Partial Internal Forces (PIFs) method (original German name is the Teilschnittgrößenverfahren (TSV) method), valid for cross-sections consisting of three rectangles [60].

Table 13. Resistances of the I 200a-section under the bending moment $M_{y.Ed}$ and bimoment B_{Ed} combination.

	Source	Quantity	Results for various u [cm] and e [cm] values						
stress-strain diagram with strengthening [53]	Streľbickaja [53]	u [cm]	5.0	4.667	3.667	2.667	1.667	0.667	0.0
		e [cm]	1.347	1.395	1.592	1.936	2.694	5.725	–
	Eq. (45)	$B_{Ed,s}$ [kNm²]	0.0	0.174	0.382	0.546	0.667	0.747	0.776
	Eq. (44)	$M_{y,Ed.s}$ [kNm]	39.10	35.29	29.74	23.96	17.82	10.62	0.0
Stress-strain diagram without strengthening [53], [71], [74], [73]	Streľbickaja Eq. (43) [53]	B_{Ed} [kNm²]	0.0	0.076	0.273	0.423	0.526	0.581	0.591
		$M_{y.Ed}$ [kNm]	30.45	28.87	24.13	19.36	14.54	9.159	0.0
	Eq. (47) [71]	$M_{y.Ed}$ [kNm]	30.50	28.93	24.20	19.46	14.69	9.92	$M_{w,Rk}$ = 6.82
	QST-TSV-3Blech programme [74]	$M_{y.Ed}$ [kNm]	29.69	28.12	23.40	18.66	13.9	9.157	0.0
	DUENQ programme [73]	$M_{y.Ed}$ [kNm]	29.0	27.5	22.6	18.0	12.9	7.6	0.0

The comparisons of the 66-year-old analytical solution [53] to the numerical results of modern computer programmes [73, 74] indicate excellent agreements (Table 13, Figure 23a) for cases without strengthening. The 66-year solution by Ukrainian lady Streľbickaja [53] is able to also contemplate strengthening, which computer programmes [73, 74] cannot do. As Equations (43)-(45) are not convenient for design standards, an interaction formula was derived by Baláž [71], which can be used in design standards, and can be written in the following different forms:

Preprints.org (www.preprints.org) | NOT PEER-REVIEWED | Posted: 6 September 2024 doi:10.20944/preprints202409.0512.v1

$$\left(\frac{M_{y,Ed}-M_{pl,y,w,Rd}}{M_{pl,y,f,Rd}}\right)^2+\frac{B_{Ed}}{B_{pl,Rd}}=1.0 \quad , \qquad M_{pl,y,Rd}=M_{pl,y,f,Rd}+M_{pl,y,w,Rd} \quad ,$$

(46)

$$M_{pl,y,w,Rd}=W_{pl,y,w}\frac{f_y}{\gamma_{M0}},\quad W_{pl,y,w}=\frac{1}{4}t_w h_w^2,\quad B_{pl,Rd}=W_{pl,\omega}\frac{f_y}{\gamma_{M0}},\quad W_{pl,\omega}=\frac{1}{4}t_f h_f b^2 \qquad (47)$$

$$\rho_{My,B}=1-\left(1-\sqrt{1-\frac{B_{Ed}}{B_{pl,Rd}}}\right)\frac{M_{pl,y,f,Rd}}{M_{pl,y,Rd}} \quad \text{if} \quad M_{y,Ed}\le M_{pl,y,w,Rd},\quad B_{Ed}=B_{pl,Rd} \qquad (48)$$

$$M_{pl,y,B,Rd}=\rho_{My,B}M_{pl,y,Rd}=M_{pl,y,Rd}-\left(1-\sqrt{1-\frac{B_{Ed}}{B_{pl,Rd}}}\right)M_{pl,y,f,Rd} \qquad (49)$$

$$\rho_{B,My}=1-\left(1-\frac{M_{pl,y,Rd}-M_{y,Ed}}{M_{pl,y,f,Rd}}\right)^2\le 1.0 \qquad (50)$$

$$B_{pl,My,Rd}=\rho_{B,My}B_{pl,Rd}=\left[1-\left(1-\frac{M_{pl,y,Rd}-M_{y,Ed}}{M_{pl,y,f,Rd}}\right)^2\right]B_{pl,Rd} \qquad (51)$$

Reduction factor $\rho_{My,B}$ provides the value by which plastic bending moment resistance $M_{y,pl,Rd}$ should be reduced for the given B_{Ed} / $B_{pl,Rd}$ and $M_{pl,y,f,Rd}$ values. Similarly, reduction factor $\rho_{B,My}$ gives the value by which plastic bimoment resistance $B_{pl,Rd}$ should be reduced for the given $M_{y,Ed}$, $M_{y,pl,Rd}$ and $M_{pl,y,f,Rd}$ values.

The plastic resistance of an I-section without strengthening is solved in [75]. The formula published in [75] has several drawbacks, which were corrected by Baláž in [76].

The form of the original formula proposed by Mirambell [75] is as follows:

$$M_{c,B,Rd}=\sqrt{1-\frac{\sigma_{w,Ed.\max}}{\frac{\alpha f_y}{4\gamma_{M0}}}}M_{c,Rd}=\sqrt{1-\frac{\sigma_{w,Ed,\max}}{\frac{5f_y}{4\gamma_{M0}}}}M_{c,Rd}=\sqrt{1-\frac{\sigma_{w,Ed,\max}}{\frac{1.25f_y}{\gamma_{M0}}}}M_{c,Rd} \qquad (52)$$

Mirambell`s formula (52) is not convenient for standard purposes because Eurocodes prefer to use internal forces, and not stresses, in formulae. Moreover, it is incorrect at first glance because for $M_{y,Ed}=0$, kNm does not give the $B_{Ed,max}=B_{pl}$ value for $\alpha=5$ and considerably differs from the exact results (Figure 23b).

Mirambell`s incorrect formula [75], which was in draft prEN 1993-1-1, was replaced with Baláž`s correct formula [76], and now appears in EN 1993-1-1:2022 [65]

$$M_{pl,y,B,Rd}=\sqrt{1-\frac{6}{\alpha}\frac{B_{Ed}}{B_{pl,Rd}}}M_{pl,y,Rd}=\rho_{My,B}M_{pl,y,Rd} \qquad (53)$$

Formula (53) gives values $\alpha=4$, 5 and 6 for maximum bimoment values $B_{Ed,max}=(4/4)\ B_{el}=(2/3)\ B_{pl}=0.667\ B_{pl}$; $B_{Ed,max}=(5/4)B_{el}=(5/6)\ B_{pl}=0.833\ B_{pl}$ and $B_{Ed,max}=(3/2)\ B_{el}=1.0\ B_{pl}$ because $B_{pl}=(3/2)$ and $B_{el}=1.5\ B_{el}$. See the ends of curves on the horizontal axis in Figure 23b.

Preprints.org (www.preprints.org) | NOT PEER-REVIEWED | Posted: 6 September 2024 doi:10.20944/preprints202409.0512.v1

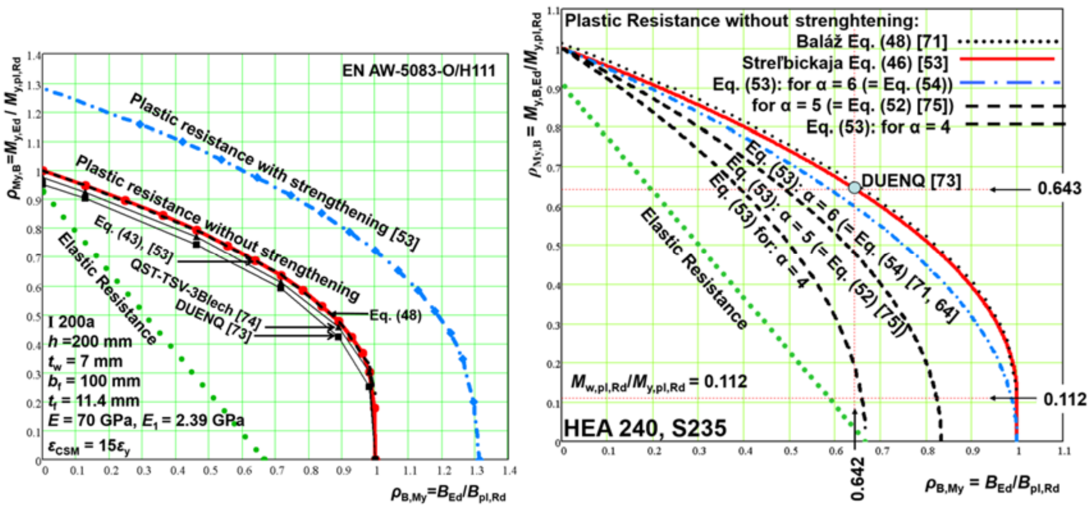

a) b)

Figure 23. The I-shaped profiles under the bending moment $M_{y,Ed}$ and bimoment B_{Ed} combination: a) the aluminium I 200a old Russian section, material: EN AW-5083-O/H111, $f_o = 110$ MPa, $f_u = 270$ MPa, $\gamma_{M1} = 1.0$, is used instead of $\gamma_{M1} = 1.1$ [64]. Elastic and plastic resistance without and with strengthening. Details of calculations based on the CSM; see [71]. W_{pl}-values appear in Figure 24a; b) the steel HEA 240 section, material: S235, f_y = 235 MPa, γ_{M0} = 1.0 [76], elastic and plastic resistance without strengthening. W_{pl}-values appear in Figure 24b.

The case with $\alpha = 6$ comes very close to the more exact solution by Streľbickaja [53] defined by Eqs. (46, 48) and is on the safe side. Eq. (53) with $\alpha = 6$, as recommended by Baláž [71, 76] for standard purposes, and was finally was accepted in EN 1993-1-1:2022 [65]:

$$M_{pl,y,B,Rd} = \sqrt{1 - \frac{B_{Ed}}{B_{pl,Rd}}} M_{pl,y,Rd} = \rho_{My,B} M_{pl,y,Rd} \tag{54}$$

The 66-year-old exact analytical solution (Eqs. (46, 48)) by Ukrainian lady Streľbickaja [53], which gives the same values as computer programme DUENQ [73], was slightly simplified by Baláž [76] for standard purposes, and finally replaced the incorrect solution [75] accepted for prEN 1993-1-1.

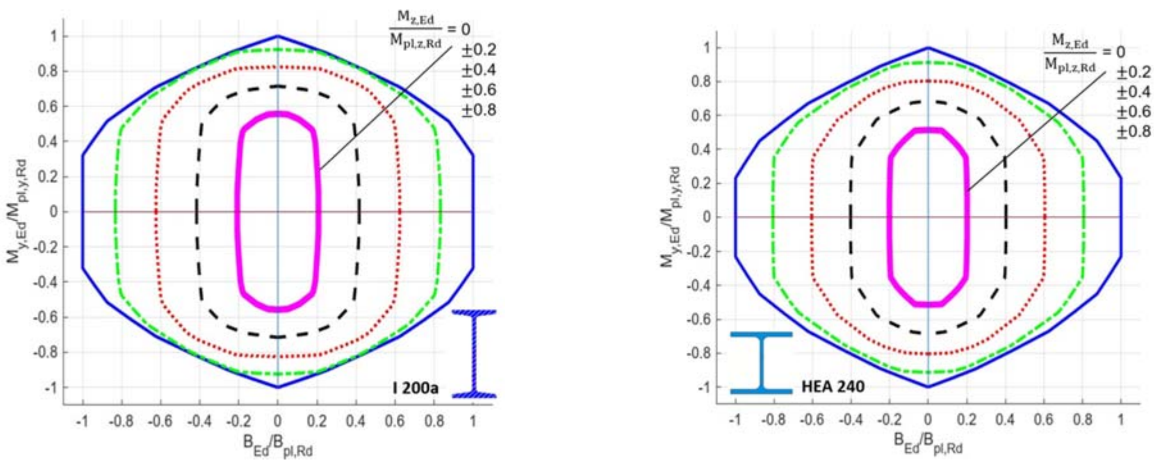

a) b)

Figure 24. Interaction diagrams $M_{y,Ed}$ + $M_{z,Ed}$ + B_{Ed} for the midline model: a) the aluminium I 200a section: A = 36.0 cm^2, $W_{pl,y}$ = 277.25 cm^3, $W_{pl,z}$ = 57.0 cm^3, $W_{pl,yw}$ = 537.51 cm^4; b) the steel HEA 240 section: A = 73.95 cm^2, $W_{pl,y}$ = 716.45 cm^3, $W_{pl,z}$ = 345.6 cm^3, $W_{pl,yw}$ = 3 767.504 cm^4.

The plastic resistance of the IPE-section without strengthening, and under the interaction of two bending internal forces $M_{y,\mathrm{Ed}}$, $V_{z,\mathrm{Ed}}$ and three torsion internal forces B_{Ed}, $T_{w,\mathrm{Ed}}$ and $T_{t,\mathrm{Ed}}$, is solved in [77].

5.4. Steel Channel Cross-Section Profile under the Moment $M_{y,Ed}$ and Bimoment B_{Ed} Combination

The Channel Cross-Section Resistance Calculation According to Strel'bickaja [53]

Strel'bickaja [53] investigated channel cross-sections in the same way as I-sections (see paragraph 5.3). The authors verified some of her analytical formulae by computer programmes [73, 74]. The comparisons once again showed Strel'bickaja's genius. Eurocodes [65-68] give plastic cross-section interaction equations for I-sections, but none for channels. The plastic resistance with strengthening in Eurocodes is not addressed at all. In the next paragraph, the authors provide results related to all three channel resistances, but only for the combination of two internal forces: bending moment $M_{y,\mathrm{Ed}}$ and negative bimoment B_{Ed}. In [53] both cases, b_1) and b_2) (Figs. 21b, 22) are solved. The a) case with positive bimoment B_{Ed} (Figure 22) is not solved in [53].

$$W_{el,y} = t_f b_f h_f + t_w h_f^2 / 6 = 1.7\,x 10.4\,x 34.3 + 1.2\,x 34.3^2 / 6 = 841.722 \text{ cm}^3, \quad (55)$$

$$W_{pl,y,\max} = t_f b_f h_f + t_w h_f^2 / 4 = 1.7\,x 10.4\,x 34.3 + 1.2\,x 34.3^2 / 4 = 959.731 \text{ cm}^3, \quad (56)$$

$$M_{el,y,Rd} = W_{el,y} f_y / \gamma_{M0} = 841.722 \text{ cm}^3\, 235 \text{ MPa} / 1. = 197.805 \text{ kNm}, \quad (57)$$

$$M_{pl,y,Rd,\max} = W_{pl,y,\max} f_y / \gamma_{M0} = 959.371 \text{ cm}^3\, 235 \text{ MPa} / 1.0 = 225.452 \text{ kNm} \quad (58)$$

Position of the shear centre in the elastic state

$$a_{y,el} = t_f h_f^2 b_f / \left(2W_{el,y}\right) = 3.746 \text{ cm} \quad (59)$$

Positions of the shear centre in the plastic state without and with strengthening, respectively

$$a_{y,pl} = t_f h_f^2 b_f / \left(2W_{pl,y}\right) = 3.287 \text{ cm}, \qquad a_{y,pl,s} = a_{y,el}\left(1+\eta_y\right) W_{el.y} / \left(W_{pl,y} + \eta_y W_{el,y}\right) = 3.37 \text{ cm}$$

(60)

The warping coordinates at the flange end and at the flange-web intersection point, respectively

$$\omega_1 = \left(b_f - a_{y,el}\right) h_f / 2 = 114.11 \text{ cm}^2, \qquad \omega_2 = a_{y,el} h_f / 2 = 64.25 \text{ cm}^2$$

(61)

$$I_w = \left[\left(b_f - a_{y,el}\right) t_f \omega_1^2 + \left(t_f h_w / 2 + t_w a_{y,el}\right) \omega_2^2\right] 2/3 = 172.4 \text{x} 10^3 \text{ cm}^6 \quad (62)$$

$$W_{el,w} = I_w / \max\left(\omega_1, \omega_2\right) = 1510 \text{ cm}^4, \quad B_{el,Rd} = W_{el,w} f_y / \gamma_{M0} = 3.549 \text{ kNm}^2 \quad (63)$$

$$W_{pl,w} = \left[t_f b_f^2 + t_f b_f h_f / 2 - t_w^2 h_f^2 / \left(16 t_f\right)\right] h_f / 4 = 2878 \text{ cm}^4,$$

$$B_{pl,Rd} = W_{pl,w} f_y / \gamma_{M0} = 6.763 \text{ kNm}^2 \quad (64)$$

(i) The elastic limit state is defined by the linear interaction formula (see Eq. (42)).

Preprints.org (www.preprints.org) | NOT PEER-REVIEWED | Posted: 6 September 2024 doi:10.20944/preprints202409.0512.v1

From Figure 21b, plastic resistances can be derived as functions of distance u when defining the position of the neutral axis in channels under the bending moment $M_{y,Ed}$ and bimoment B_{Ed} combination. For the plastic limit state:
(ii) without strengthening $\eta_y = 0$ (Figure 20). Formulae (65) are the formulae (38.26) in [53]:

$$M_{y,Ed}(u) = \left[(2u-b)t_f h_f + t_w h_f^4/4\right] f_y, \quad B_{Ed}(u) = M_{y,Ed}(u) a_{y,pl} + \left(\frac{b_f^2}{2} - u^2\right) t_f h_f f_y \qquad (65)$$

(iii) with strengthening $\eta_y = 0.25$ (Figure 20):
for the b_1 case (Figure 21b):

$$M_{y,Ed,s}(u) = M_{y,Ed}(u) + \left[W_{el,y} - t_f h_f b_f^2/(2u)\right]\eta_y f_y \qquad (66)$$

$$B_{Ed,s}(u) = M_{y,Ed}(u) a_{y,pl,s} + \left(\frac{b_f^2}{2} - u^2\right) t_f h_f f_y + \left[2b_f^3/(3u) - b_f^2\right]\eta_y f_y t_f h_f/2 \qquad (67)$$

for the b_2 case (Figure 21b):

$$M_{y,Ed,s}(u) = M_{y,Ed}(u) + \left[uW_{el,y} - t_f h_f b_f^2/2\right]\eta_y f_y/(b_f - u) \qquad (68)$$

$$B_{Ed,s}(u) = M_{y,Ed}(u) a_{y,pl,s} + \left(\frac{b_f^2}{2} - u^2\right) t_f h_f f_y + (2b_f/3 - u)\eta_y f_y t_f h_f b_f^2/\left[(b_f - u)2\right] \qquad (69)$$

For $u = b_f/2$, Eqs. (68) and (69) equal Eqs. (66) and (67).

In this paper, the results of analytical solution [53] for the b) case (negative B_{Ed}, Figs. 21b, 22) are presented and compared to the computer programme results [74]. For the a) case (positive B_{Ed}, Figure 22), only the computer programme results [74] are shown.

The obtained results and comparisons of the analytical [53] and computer results [74] are graphically presented in Figure 25. Comparisons show acceptable agreements between these results. For the negative bimoment (b) case in Figs. 21, 22), the final result is the simple interaction formula (70) derived by Baláž [71] on the basis of Streľbitskaja's results [53]. Eq. (70) is limited to $M_{y,Ed} \le M_{pl,y,Rd}$ and is on the safe side. Compare the solid line right end to the numerical results for the "full black circles" obtained by the computer programme [74] (see Figure 25).

$$\frac{B_{Ed}}{B_{pl,Rk}} = K_1\left(\frac{M_{y,Ed}}{M_{pl,y,Rk}}\right)^2 - K_2\frac{M_{y,Ed}}{M_{pl,y,Rk}} - 1 \qquad (70)$$

where

$$K_1 = (4a_{wf}+1)^2/(16a_{wf}^2 + 8a_{wf} - 1),\ K_2 = 2/(16a_{wf}^2 + 8a_{wf} - 1),\ a_{wf} = A_f/A_w = b_f t_f/(h_f t_w) \qquad (71)$$

It is interesting to show: (i) the $B_{Ed,conc}$ value associated (concomitant) with maximum bending moment $M_{pl,y,Rd,max}$; (ii) value $M_{Ed,conc}$ associated (concomitant) with maximum bimoment $B_{pl,Rd,max} > B_{pl,Rd}$. See the diagram for the plastic resistance without strengthening in Figure 25. Both computer programmes DUENQ [73] and QST-TSV-3Blech [74] offer similar values, which are presented in Table 14.

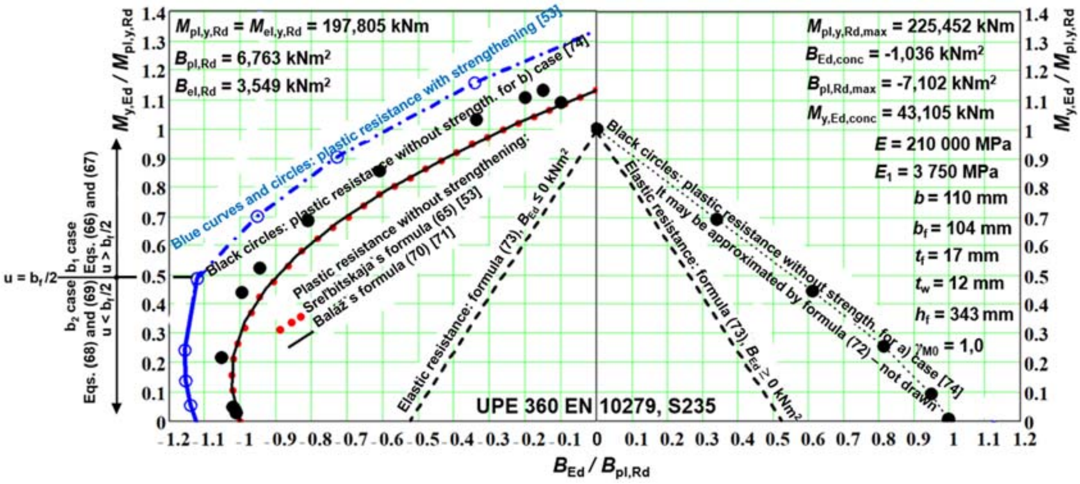

Figure 25. – Comparison of channel resistances, the results of different calculation ways. To the right of the figure there is the quadrant for the $+M_{yd,Ed}$ and $+B_{Ed}$ combination. To the left part of the figure lies the quadrant for the $+M_{yd,Ed}$ and $-B_{Ed}$ combination. Compare these two quadrants to the upper part of Figure 26, where all four quadrants include combinations $-M_{yd,Ed}$ with $-B_{Ed}$ and $-M_{yd,Ed}$ with $+B_{Ed}$ seen in the bottom diagram part in Figure 26.

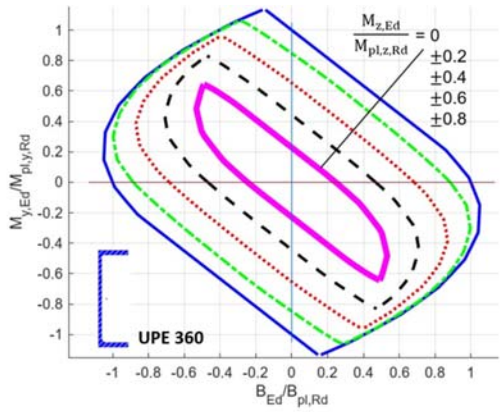

Figure 26. The UPE 360 section. Interaction diagrams $M_{y,Ed} + M_{z,Ed} + B_{Ed}$. For the midline model: $N_{pl,Rd}$ = 1798 kN, $M_{pl,y,Rd}$ = 197.80 kNm, $M_{pl,z,Rd}$ = 44.24 kNm, , $B_{pl,Rd}$ = 6.795 kNm², $M_{pl,y,Rd,max}$ = 225.45 kNm with $B_{Ed,conc}$ = -1.0357 kNm², $B_{pl,Rd,max}$ = -7.3304 kNm² with $M_{y,Ed,conc}$ = 47.31 kNm. Compare these values to the results in Table 14.

Table 14. The UPE 360 section plastic resistances without strengthening for negative bimoment B_{Ed} (case b) in Figs. 21b, 22). Compare these results to the values in Figures 18a, b and 26.

Computer programmes	Maximum internal force	The corresponding value
QST-TSV-3Blech [74]	$M_{pl,y,Rd,max}$ = 225.452 kNm	$B_{Ed,Mmax} = B_{Ed,conc}$ = -1.0144 kNm²
DUENQ [73]		$B_{Ed,Mmax} = B_{Ed,conc} \approx$ -1.0500 kNm²
QST-TSV-3Blech [74]	$B_{pl,Rd,max}$ = Rd,maxBlech ² > $B_{pl,Rd}$ = 6.763 kNm²	$M_{Ed,Bmax} = M_{Ed,conc}$ = 43.31 kNm
DUENQ [73]	$B_{pl,Ed,max}$ l,Ed,max]mmch ² > $B_{pl,Rd}$ = 6.763 kNm²	$M_{Ed,Bmax} = M_{Ed,conc}$,conc kNmmc
QST-TSV-3Blech [74]	$M_{pl,y,Rd}$ = 199.52 kNm	$B_{Ed,Mpl} = B_{Ed,conc}$ = 0 kNm²
DUENQ [73]	$M_{pl,y,Rd}$ = 192.00 kNm	

For the positive bimoment (a) case in Figure 22, the linear interaction formula defined by Eq. (72) can be used (see the left-hand part of Figure 25) and are on the safe side:

Preprints.org (www.preprints.org) | NOT PEER-REVIEWED | Posted: 6 September 2024 doi:10.20944/preprints202409.0512.v1

$$\frac{M_{\mathrm{y,Ed}}}{M_{\mathrm{pl,y,Rd}}}+\frac{B_{\mathrm{Ed}}}{B_{\mathrm{pl,Rd}}}\leq 1.0 \qquad (72)$$

For the investigated UPE 360, formula (72) can be used within the interval $-0.1 \leq B_{\mathrm{Ed}}/B_{\mathrm{pl,Rd}} \leq 1.0$ and formula (70), after multiplication by factor -1.0, can be used within the interval $-1.0 \leq B_{\mathrm{Ed}}/B_{\mathrm{pl,Rd}} \leq -0.1$.

As part of the large parametrical study, the other UPE-section sizes were also investigated. The obtained results confirmed the possibility of using for channels the simple interaction formulae defined by Eq. (70) and Eq. (72), derived for standard purposes.

The elastic limit state is defined by linear interaction formula (42). The graphical interpretation of Eq. (42) in Figure 25 can be described as follows:

$$\frac{M_{\mathrm{y,Ed}}}{M_{\mathrm{el,y,Rd}}}\pm\frac{B_{\mathrm{Ed}}}{B_{\mathrm{el,Rd}}}\leq 1.0,\quad M_{\mathrm{el,y,Rd}}=M_{\mathrm{pl,yRd}},\quad B_{\mathrm{el,Rd}}=0.525B_{pl,Rd},\quad \frac{M_{\mathrm{y,Ed}}}{M_{\mathrm{pl,y,Rd}}}\pm\frac{B_{\mathrm{Ed}}}{0.525B_{\mathrm{pl,Rd}}}\leq 1.0 \qquad (73)$$

The following Tables 15a,b – 17a,b contain the formulae of all the cross-sectional properties for a) the monosymmetric I-shaped section, b) the channel and c) the Z-section, including relevant concomitant internal forces. The calculation of approximate values is based on the midline model with thicknesses by taking into account details (a) + (d) of element connections (Figure 4). Formulae are presented in both the a) dimensionless form to enable parametrical studies and b) the formulae for direct designs. They are proposed for educational purposes and also for quick structures design in practice. W_{pl} values relate to the fibres located on the midline, and not to the section surface.

The symbols used in Table 15a:

$$b_{ub}=\frac{b_u}{b_b},\quad t_{ub}=\frac{t_u}{t_b},\quad A_{ub}=\frac{A_u}{A_b}=\frac{b_u t_u}{b_b t_b},\quad A_{wb}=\frac{A_w}{A_b}=\frac{h_f t_w}{b_b t_b},\quad h_f=h-\frac{t_u+t_b}{2}. \qquad (74)$$

Table 15a. The monosymmetric I-shaped section's plastic properties.

Relative plastic section moduli $\overline{W}_{pl}(b_{ub},t_{ub},A_{ub},A_{wb})$	Plastic section moduli W_{pl}
$\overline{W}_{pl,y}=\dfrac{W_{pl,y}}{b_u t_u h_f}=\dfrac{1}{A_{ub}}+\dfrac{A_{wb}}{2A_{ub}}$, if $\dfrac{1+A_{wb}}{A_{ub}}<1$, $\overline{W}_{pl,y}=\dfrac{W_{pl,y}}{b_u t_u h_f}=1+\dfrac{A_{wb}}{2A_{ub}}$, if $A_{ub}+A_{wb}<1$, otherwise: $\overline{W}_{pl,y}=\dfrac{W_{pl,y}}{b_u t_u h_f}=\dfrac{(A_{ub}+A_{wb})^2+2(A_{ub}-A_{ub}^2+A_{wb})-1}{4A_{ub}A_{wb}}$	$W_{pl,y}=\left(\dfrac{1}{A_{ub}}+\dfrac{A_{wb}}{2A_{ub}}\right)b_u t_u h_f$, if $\dfrac{1+A_{wb}}{A_{ub}}<1$ $W_{pl,y}=\left(1+\dfrac{A_{wb}}{2A_{ub}}\right)b_u t_u h_f$, if $A_{ub}+A_{wb}<1$ $W_{pl,y}=\overline{W}_{pl,y}b_u t_u h_f$, otherwise
$\overline{W}_{pl,y,\max}=\dfrac{W_{pl,y,\max}}{b_u t_u h_f}=\dfrac{\left(2+\dfrac{A_{wb}}{A_{ub}}\right)(2+A_{wb})(2+2A_{ub}+A_{wb})}{4(1+A_{ub}+A_{wb})^2}$	$W_{pl,y,\max}=\overline{W}_{pl,y,\max}b_u t_u h_f$

$\overline{W}_{pl,z} = \frac{W_{pl,z}}{0.25b_b^2 t_b} = 1 + b_{ub}^3 t_{ub}$, if $b_{ub} < 1$, $\overline{W}_{pl,z} = \frac{W_{pl,z}}{0.25b_b^2 t_b} = \frac{1}{b_{ub}} + b_{ub}^2 t_{ub}$, if $1 \le b_{ub}$	$W_{pl,z} = \left(1 + b_{ub}^3 t_{ub}\right)\frac{b_b^2 t_b}{4}$, if $b_{ub} < 1$, $W_{pl,z} = \left(\frac{1}{b_{ub}} + b_{ub}^2 t_{ub}\right)\frac{b_b^2 t_b}{4}$, if $1 \le b_{ub}$
$\overline{W}_{pl,z,\max} = \frac{W_{pl,z,\max}}{0.25b_b^2 t_b} = 1 + b_{ub}^2 t_{ub}$	$W_{pl,z,\max} = \left(1 + b_{ub}^2 t_{ub}\right)\frac{b_b^2 t_b}{4}$
$\overline{W}_{pl,w} = \frac{W_{pl,w}}{0.25b_u^2 t_u h_f} = \frac{1}{b_{ub}^2 t_{ub}}$, if $1 \le b_{ub}^2 t_{ub}$, $\overline{W}_{pl,w} = \frac{W_{pl,\omega}}{0.25b_u^2 t_u h_f} = 1$, if $b_{ub}^2 t_{ub} < 1$	$W_{pl,w} = \frac{1}{b_{ub}^2 t_{ub}} \frac{b_u^2 t_u h_f}{4}$, if $1 \le b_{ub}^2 t_{ub}$, $W_{pl,w} = \frac{b_u^2 t_u h_f}{4}$, if $b_{ub}^2 t_{ub} < 1$
$\overline{W}_{pl,w,\max} = \frac{W_{pl,w,\max}}{0.25b_u^2 t_u h_f} = \frac{1 + b_{ub}}{1 + b_{ub}^3 t_{ub}}$	$W_{pl,w,\max} = \frac{1 + b_{ub}}{1 + b_{ub}^3 t_{ub}} \frac{b_u^2 t_u h_f}{4}$
Combination of maximum bending moment $M_{pl,z.Ed,\max}$ with concomitant bimoment $B_{Ed,conc}$: $M_{pl,z,Ed,\max} = W_{pl,z,\max} f_y$, $B_{Ed,conc} = \frac{1 - b_{ub}}{1 + b_{ub}^3} \frac{b_u^2 t_u}{4} h_f f_y$	
Combination of maximum bimoment $B_{pl,Ed,\max}$ with concomitant bending moment $M_{z,Ed,conc}$: $B_{pl,Ed,\max} = W_{pl,w,\max} f_y$, $M_{z,Ed,conc} = \left(b_{ub}^2 t_{ub} - 1\right)\frac{b_b^2 t_b}{4} h_f f_y$	
Combination of maximum bimoment $M_{pl,y,Ed,\max}$ with concomitant axial force $N_{Ed,conc}$: $M_{pl,y,Ed,\max} = W_{pl,y,\max} f_y$, $N_{Ed,conc} = \frac{A_{ub}^2 - 1}{\left(1 + A_{ub} + A_{wb}\right)^2} b_u t_u f_y$	

Table 15b. The monosymmetric I-shaped section's properties.

Preprints.org (www.preprints.org) | NOT PEER-REVIEWED | Posted: 6 September 2024 doi:10.20944/preprints202409.0512.v1

$$h_f = h - \frac{t_u + t_b}{2}, \quad b_{ub} = \frac{b_u}{b_b}, \quad t_{ub} = \frac{t_u}{t_b}, \quad A_{ub} = \frac{A_u}{A_b} = \frac{b_u t_u}{b_b t_b}, \quad A_{wb} = \frac{A_w}{A_b} = \frac{h_f t_w}{b_b t_b},$$

$$A = A_u + A_w + A_b, \quad I_u = \frac{1}{12} A_u b_u^2, \quad I_b = \frac{1}{12} A_b b_b^2, \quad I_z = I_u + I_b, \quad \varphi = \frac{A_u - A_b}{A},$$

$$\psi = \frac{I_u - I_b}{I_z},$$

$$z_{Gu} = (1-\varphi)\frac{h_f}{2}, \quad z_{Gb} = (1+\varphi)\frac{h_f}{2}, \quad z_{GS} = (\psi - \varphi)\frac{h_f}{2}, \quad z_{Su} = (1-\psi)\frac{h_f}{2}, \quad z_{Sb} = (1+\psi)\frac{h_f}{2},$$

$$\omega_u = \pm z_{Su}\frac{b_u}{2} = \pm \frac{A_b b_b^2}{A_u b_u^2 + A_b b_b^2}\frac{b_u h_f}{2}, \quad \omega_b = \mp z_{Sb}\frac{b_b}{2} = \mp \frac{A_u b_u^2}{A_u b_u^2 + A_b b_b^2}\frac{b_b h_f}{2},$$

$$I_y = \left(1-\varphi^2\right)\frac{A h_f^4}{4} - \frac{A_w h_f^2}{6} = \frac{12 A_{ub} + 4 A_{ub} A_{wb} + 4 A_{wb} + A_{wb}^2}{12\left(1 + A_{ub} + A_{wb}\right)} A_u h_f^2,$$

$$I_w = \left(1-\psi^2\right)\frac{I_z h_f^2}{4} = \omega_u^2 \frac{A_u}{3} + \omega_b^2 \frac{A_b}{3},$$

$$W_{el,y} = \frac{I_y}{\max\left(|z_{Gu}|, |z_{Gb}|\right)}, \quad W_{el,z} = \frac{I_z}{0.5\max\left(b_u, b_b\right)}, \quad W_{el,w} = \frac{I_w}{\max\left(|\omega_u|, |\omega_b|\right)},$$

$$z_j = \left[\psi\left(1 - \frac{I_z}{2 I_y}\right) - \varphi\left(\frac{A_w h_f^2 - 6 I_z}{12 I_y}\right)\right]\frac{h_f}{2}$$

Table 16a. The channel section's plastic properties. $A_f = b_w t_f$, $A_w = h_f t_w$, $\alpha_{fw} = \dfrac{A_f}{A_w}$.

Relative plastic section moduli. $\overline{W}_{pl}(\alpha_{fw})$	Plastic section moduli W_{pl}
$\overline{W}_{pl,y} = \overline{W}_{el,y} = \dfrac{W_{pl,y}}{h_f A_w} = \dfrac{1}{6} + \alpha_{fw}$	$W_{pl,y} = W_{el,y} = \left(\dfrac{1}{6} + \alpha_{fw}\right) h_f A_w$
$\overline{W}_{pl,y,\max} = \dfrac{W_{pl,y,\max}}{h_f A_w} = \dfrac{1}{4} + \alpha_{fw}$	$W_{pl,y,\max} = \left(\dfrac{1}{4} + \alpha_{fw}\right) h_f A_w$
$\overline{W}_{pl,z} = \dfrac{W_{pl,z}}{b_w A_f} = \dfrac{1}{2}\left(1 + \dfrac{1}{\alpha_{fw}} - \dfrac{1}{4\alpha_{fw}^2}\right)$, if $2\alpha_{fw} \geq 1$	$W_{pl,z} = \dfrac{1}{2}\left(1 + \dfrac{1}{\alpha_{fw}} - \dfrac{1}{4\alpha_{fw}^2}\right) b_w A_f$, $2\alpha_{fw} \geq 1$

 doi:10.20944/preprints202409.0512.v1

$\overline{W}_{pl,z} = \dfrac{W_{pl,z}}{b_w A_w} = \alpha_{fw}$, if $2\alpha_{fw} < 1$	$W_{pl,z} = \alpha_{fw} b_w A_w$, if $2\alpha_{fw} < 1$
$\overline{W}_{pl,z,\max} = \dfrac{2(1+\alpha_{fw})^2}{(1+2\alpha_{fw})^2}$	$W_{pl,z,\max} = \dfrac{2(1+\alpha_{fw})^2}{(1+2\alpha_{fw})^2} b_w A_f$
$\overline{W}_{pl,w} = \dfrac{W_{pl,w}}{b_w h_f A_f} = \left(\dfrac{1}{4} + \dfrac{1}{8\alpha_{fw}} - \dfrac{1}{64\alpha_{fw}^2}\right)$, $4\alpha_{fw} \geq 1$ $\overline{W}_{pl,w} = \dfrac{W_{pl,w}}{b_w h_f A_f} = \dfrac{1}{2}$, if $4\alpha_{fw} \leq 1$	$W_{pl,w} = \left(\dfrac{1}{4} + \dfrac{1}{8\alpha_{fw}} - \dfrac{1}{64\alpha_{fw}^2}\right) b_w h_f A_f$, if $4\alpha_{fw} \geq 1$ $W_{pl,w} = \dfrac{1}{2} b_w h_f A_f$, if $4\alpha_{fw} \leq 1$
$\overline{W}_{pl,w,\max} = \dfrac{W_{pl,w,\max}}{b_w h_f A_f} = \dfrac{5+30\alpha_{fw}+36\alpha_{fw}^2}{4(1+6\alpha_{fw})^2}$	$W_{pl,w,\max} = \dfrac{5+30\alpha_{fw}+36\alpha_{fw}^2}{4(1+6\alpha_{fw})^2} b_w h_f A_f$
Combination of maximum plastic bending moment $M_{pl,y,Ed,\max}$ with concomitant bimoment $B_{Ed,conc}$: $M_{pl,y,Ed,\max} = W_{pl,y,\max} f_y$, $B_{Ed,conc} = \dfrac{1}{4(1+6\alpha_{fw})} b_w h_f A_f f_y$	
Combination of maximum plastic bimoment $B_{pl,Ed,\max}$ with concomitant bending moment $M_{y,Ed,conc}$: $B_{pl,Ed,\max} = W_{pl,w,\max} f_y$, $M_{y,Ed,conc} = \dfrac{1+2\alpha_{fw}}{4(1+6\alpha_{fw})} h_f A_w f_y$	
Combination of maximum plastic bending moment $M_{pl,z,Ed,\max}$ with concomitant axial force $N_{Ed,conc}$: $M_{pl,z,Ed,\max} = W_{pl,z,\max} f_y$, $N_{Ed,conc} = \dfrac{1}{1+2\alpha_{fw}} h_f t_w f_y$	

Table 16b. The channel section's properties.

 doi:10.20944/preprints202409.0512.v1

$$A_f = b_w t_f\,,\quad A_w = h_f t_w\,,\quad \alpha_{fw} = \frac{A_f}{A_w}\,,\quad A = 2A_f + A_w\,,\quad I_f = \frac{1}{12}A_f b_w^2\,,\quad I_{we} = \frac{1}{12}A_w h_f^2\,,$$

$$\varphi = \frac{A_w}{A}\,,\quad \psi = \frac{3(1-\varphi)}{3-2\varphi}\,,\quad y_{Gw} = (1-\varphi)\frac{b_w}{2} = \frac{\alpha_{fw}}{1+2\alpha_{fw}}b_w\,,\quad y_{Gf} = (1+\varphi)\frac{b_w}{2} = \frac{1+\alpha_{fw}}{1+2\alpha_{fw}}b_w\,,$$

$$e = \frac{3\alpha_{fw}}{1+6\alpha_{fw}}b_w\,,\quad \omega_w = \pm\frac{e}{2}h_f = \pm\frac{3\alpha_{fw}}{2(1+6\alpha_{fw})}b_w h_f\,,\quad \omega_f = \mp\frac{b_w - e}{2}h_f = \mp\frac{1+3\alpha_{fw}}{2(1+6\alpha_{fw})}b_w h_f\,,$$

$$y_{GS} = \frac{1+\psi-\varphi}{2}b_w = \frac{4\alpha_{fw}(1+3\alpha_{fw})}{(1+2\alpha_{fw})(1+6\alpha_{fw})}b_w\,,$$

$$I_y = \frac{1}{1-\psi}I_{we} = (1+6\alpha_{fw})I_{we}\,,\quad W_{el,y} = \left(\frac{1}{6}+\alpha_{fw}\right)h_f A_w\,,$$

$$I_z = (1+3\varphi)2I_f = 4(1+6\alpha_{fw})I_f\,,\quad W_{el,z} = \frac{2+\alpha_{fw}}{3(1+\alpha_{fw})}b_w A_f\,,$$

$$I_w = \psi(4-3\psi)\frac{b_w^2}{12}I_y = \frac{2+3\alpha_{fw}}{12(1+6\alpha_{fw})}b_w^2 h_f^2 A_f\,,\quad W_{el,w} = \frac{2+3\alpha_{fw}}{6(1+3\alpha_{fw})}b_w h_f A_f\,,$$

$$y_j = \pm y_{GS} \mp \frac{1}{2I_z}\int_A (y^2+z^2)y\,dA = \left(1+\psi-\frac{\varphi}{1+3\varphi}-\frac{1-\psi-\varphi}{2}\frac{I_y}{I_z}\right)\frac{b_w}{2} =$$

$$= \frac{3+4\alpha_{fw}(11+6\alpha_{fw})+(1+6\alpha_{fw})\left(\frac{h_f}{b_w}\right)^2}{4(2+\alpha_{fw})(1+6\alpha_{fw})}b_w$$

e is the horizontal distance of the shear centre from the web midline,

y_{Gw} is the horizontal distance of the gravity centre from the web midline,

y_{Gf} is the horizontal distance of the gravity centre from the flange tip,

y_{GS} is the horizontal distance of the shear centre from the gravity centre,

y_j is the monosymmetry parameter

Table 17a. The Z-section's plastic properties. $A_f = b_w t_f\,,\ A_w = h_f t_w\,,\ \alpha_{fw} = \dfrac{A_f}{A_w}$.

Relative plastic section moduli $\overline{W}_{pl}(\alpha_{fw})$	Plastic section moduli W_{pl}

$\overline{W}_{pl,y} = \dfrac{W_{pl,y}}{h_f A_w} = \dfrac{1}{4} + \left(\sqrt{2}-1\right)\alpha_{fw}$	$W_{pl,y} = \left[\dfrac{1}{4} + \left(\sqrt{2}-1\right)\alpha_{fw}\right] h_f A_w$
$\overline{W}_{pl,y,\max} = \dfrac{W_{pl,y,\max}}{h_f A_w} = \dfrac{1}{4} + \alpha_{fw}$	$W_{pl,y,\max} = \left(\dfrac{1}{4} + \alpha_{fw}\right) h_f A_w$
$\overline{W}_{pl,z} = \dfrac{W_{pl,z}}{b_w A_f} = \dfrac{1}{2}\left(1 + \dfrac{1}{2\alpha_{fw}} - \dfrac{1}{16\alpha_{fw}^2}\right)$	$W_{pl,z} = \dfrac{1}{2}\left(1 + \dfrac{1}{2\alpha_{fw}} - \dfrac{1}{16\alpha_{fw}^2}\right) b_w A_f$
$\overline{W}_{pl,z,\max} = \dfrac{W_{pl,z,\max}}{b_w A_f} = 1$	$W_{pl,z,\max} = b_w A_f$
$\overline{W}_{pl,w} = \dfrac{W_{pl,w}}{b_w h_f A_f} = \dfrac{\left(4\alpha_{fw}-1\right)\left(1+\alpha_{fw}\right)^2}{9\alpha_{fw}^2\left(1+2\alpha_{fw}\right)}$, if $2\alpha_{fw} \geq 1$ $\overline{W}_{pl,w} = \dfrac{W_{pl,w}}{b_w h_f A_f} = \dfrac{1}{2}$, if $2\alpha_{fw} \leq 1$	$W_{pl,w} = \dfrac{\left(4\alpha_{fw}-1\right)\left(1+\alpha_{fw}\right)^2}{9\alpha_{fw}^2\left(1+2\alpha_{fw}\right)} b_w h_f A_f$, if $2\alpha_{fw} \geq 1$ $W_{pl,w} = \dfrac{1}{2} b_w h_f A_f$, if $2\alpha_{fw} \leq 1$
$\overline{W}_{pl,w,\max} = \dfrac{W_{pl,w,\max}}{b_w h_f A_f} = \left(\dfrac{1+\alpha_{fw}}{1+2\alpha_{fw}}\right)^2$	$W_{pl,w,\max} = \left(\dfrac{1+\alpha_{fw}}{1+2\alpha_{fw}}\right)^2 b_w h_f A_f$
Combination of maximum plastic bimoment $B_{pl,Ed,\max}$ with concomitant axial force $N_{Ed,conc}$: $B_{pl,Ed,\max} = W_{pl,w,\max} f_y$, $N_{Ed,conc} = \dfrac{1}{\left(1+2\alpha_{fw}\right)^2} A f_y$	
The maximum plastic bending moment about *y-y* axis $M_{pl,y,Ed,\max} = W_{pl,y,\max} f_y$ is concomitant with the maximum plastic bending moment about *z-z* axis $M_{pl,z,Ed,\max} = W_{pl,z,\max} f_y$.	

Table 17b. The Z-section's properties.

$A_f = b_w t_f$, $A_w = h_f t_w$, $A = A_w + 2A_f$, $\alpha_{fw} = \dfrac{A_f}{A_w}$, $y_{fu} = -b_w$, $z_{fu} = -\dfrac{h_f}{2}$, $y_{fb} = b_w$, $z_{fb} = \dfrac{h_f}{2}$,

$y_{fu} = -b_w$, $z_{fu} = -\dfrac{h_f}{2}$, $y_{fb} = b_w$, $z_{fb} = \dfrac{h_f}{2}$, $y_{wu} = 0$, $z_{wu} = -\dfrac{h_f}{2}$, $y_{wb} = 0$, $z_{wb} = \dfrac{h_f}{2}$,

Preprints.org (www.preprints.org) | NOT PEER-REVIEWED | Posted: 6 September 2024 doi:10.20944/preprints202409.0512.v1

Note: for indices fu, fb, wu and wb, see the locations of points in the Z-section figure (b – bottom, u – upper).

$$\omega_{we} = \pm\frac{\alpha_{fw}}{2(1+2\alpha_{fw})} b_w h_f, \qquad \omega_f = \mp\frac{1+\alpha_{fw}}{2(1+2\alpha_{fw})} b_w h_f,$$

$$I_y = \frac{1}{2}\left(\alpha_{fw} + \frac{1}{6}\right) h_f^2 A_w, \quad I_z = \frac{2}{3} b_w^2 A_f, \quad I_{yz} = \frac{1}{2} b_w h_f A_f, \quad I_w = \frac{2+\alpha_{fw}}{12(1+2\alpha_{fw})} b_w^2 h_f^2 A_f,$$

$$\overline{W}_{el,y,f} = \frac{W_{el,y,f}}{h_f A_w} = \frac{2+3\alpha_{fw}}{6}, \qquad W_{el,y,f} = \frac{2+3\alpha_{fw}}{6} h_f A_w,$$

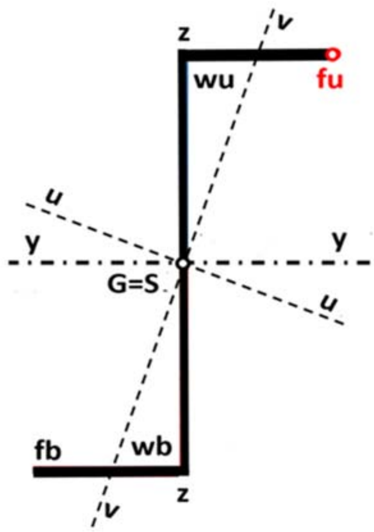

$$\overline{W}_{el,y,we} = \frac{W_{el,y,w}}{h_f A_w} = \frac{2+3\alpha_{fw}}{12},$$

$$W_{el,y,we} = \frac{2+3\alpha_{fw}}{12} h_f A_w,$$

$$\overline{W}_{el,z,f} = \frac{W_{el,z,f}}{b_w A_f} = \frac{2+3\alpha_{fw}}{3(1+3\alpha_{fw})},$$

$$W_{el,z,f} = \frac{2+3\alpha_{fw}}{3(1+3\alpha_{fw})} b_w A_f,$$

$$\overline{W}_{el,z,we} = \frac{W_{el,z,we}}{b_w A_f} = \frac{2+3\alpha_{fw}}{9},$$

$$W_{el,z,we} = \frac{2+3\alpha_{fw}}{9} b_w A_w,$$

$$\overline{W}_{el,w,f} = \frac{W_{el,w,f}}{b_w A_f} = \frac{2+\alpha_{fw}}{6(1+\alpha_{fw})}, \qquad W_{el,w,f} = \frac{2+\alpha_{fw}}{6(1+\alpha_{fw})} b_w h_f A_f,$$

$$\overline{W}_{el,w,we} = \frac{W_{el,w,we}}{b_w A_f} = \frac{2+\alpha_{fw}}{6}, \qquad W_{el,w,we} = \frac{2+\alpha_{fw}}{6} b_w h_f A_f,$$

Note: indices w – warping (except b_w, y_{wu}, y_{wb}); we – web.

$$\alpha = \frac{1}{2}\operatorname{atan}\left(\frac{2I_{yz}}{I_z - I_y}\right), \qquad u(s) = y(s)\cos(\alpha) + z(s)\sin(\alpha),$$

$$v(s) = z(s)\cos(\alpha) - y(s)\sin(\alpha),$$

$$I_u = \frac{I_y + I_z}{2} + \frac{1}{2}\sqrt{(I_y - I_z)^2 + 4I_{yz}^2},$$

$$I_v = \frac{I_y + I_z}{2} - \frac{1}{2}\sqrt{(I_y - I_z)^2 + 4I_{yz}^2},$$

Preprints.org (www.preprints.org) | NOT PEER-REVIEWED | Posted: 6 September 2024 doi:10.20944/preprints202409.0512.v1

$$C_1 = 2\alpha_{fw}\left(\frac{b_w}{h_f}\right)^2, \quad C_2 = \frac{1}{4}\left(1+6\alpha_{fw}\right),$$

$$I_u = \frac{1}{6}\left[C_1 + C_2 + \sqrt{C_1^2 + C_2^2 + \left(3\alpha_{fw}^2 - \alpha_{fw}\right)\left(\frac{b_w}{h_f}\right)^2}\,\right] h_f^2 A_w, \qquad W_{el,u} = \frac{I_u}{v_{\max}},$$

$$I_v = \frac{1}{6}\left[C_1 + C_2 - \sqrt{C_1^2 + C_2^2 + \left(3\alpha_{fw}^2 - \alpha_{fw}\right)\left(\frac{b_w}{h_f}\right)^2}\,\right] h_f^2 A_w, \qquad W_{el,v} = \frac{I_v}{u_{\max}}$$

6. Conclusions

The beginning of the "Plastic Design" development during period 1914-1959 and plastic design development pioneers are described in the Introduction. Unknown important Russian [14 – 16, 19, 21, 23, 24, 35, 40, 41, 44, 49] and Ukrainian [17, 53] achievements from this period are also mentioned. All these studies have revealed possibilities for using plastic (maximum) strength as a basis for structural design. The application of plastic design is justified for offering a satisfactory explanation of steel structures' observed ultimate strength.

The advantages of the plastic analysis and assumptions for plastic analysis applications are explained together with the metal Eurocodes requirements for the global plastic analysis of both steel structures according to EN 1993-1-1:2022 [65] and aluminium structures according to EN 1999-1-1:2023 [67].

The need to distinguish among three kinds of plastic section moduli calculated: a) without considering bimoment B_{Ed} a constraint $W_{pl,nB}$, b) considering bimoment B_{Ed} a constraint W_{pl} and c) the maximum $W_{pl,max}$ values is explained in Chapter 3 Basis of theory and in the several illustrative numerical examples.

The results of this large parametrical study focus on 18 metal thin-walled cross-sections of various shapes: doubly symmetric, monosymmetric with axis of symmetry z, monosymmetric with axis of symmetry y, point symmetric and asymmetric open and closed cross-sections. They appear in Tables 11 and 12. The values of the different plastic section moduli are obtained by distinct calculation ways using own computer programmes: a) created in MathCad; b) https://laboratoriosvirtuales.upv.es/webapps/thinwallsectiongeneral.html and c) https://labmatlab-was.upv.es/webapps/home/thinwallsectionopenclosed.html, and with d) approximate formulae for I-shaped, channel and Z-sections offered for educational purposes and the design of thin-walled structures in practice (Tables 15a,b – 17a,b). The comparisons of values show excellent agreements and the correctness of the results. Two of the above freely available own programmes (mentioned in b) and c)) allow the plastic design of thin-walled cross-sections with any open or closed shape, under any combination of eight internal forces (N_{Ed}, $M_{y,Ed}$, $M_{z,Ed}$, B_{Ed}, $V_{z,Ed}$, $V_{y,Ed}$, $T_{t,Ed}$ and $T_{w,Ed}$), to be solved.

Altogether 15 interaction diagrams present the results for various cross-section shapes under the combinations of three internal forces: $N_{Ed} + M_{y,Ed} + M_{z,Ed}$ or $M_{y,Ed} + B_{Ed} + M_{z,Ed}$. They are the product of the freely available own programmes found in this blog: https://antonioagueroramonllin.blogs.upv.es/ .

The following cross-sections loaded by various combinations of internal forces are detailed and analysed in the numerical examples: a) HEB 280 under $N_{Ed} + M_{y,Ed}$ combination (Figs. 14, 15) and under the $N_{Ed} + M_{y,Ed} + M_{z,Ed}$ combination (Figs. 16a, 16b); b) UPE 360 under $M_{y,Ed}$ (Figure 17), $N_{Ed} + M_{y,Ed} + M_{z,Ed}$ (Figs. 18a, 18b), $M_{y,Ed} + B_{Ed}$ (Figure 25, Table 14) and $M_{y,Ed} + M_{z,Ed} + B_{Ed}$ (Figure 26, Table 14); c) HEA 240 under $M_{y,Ed} + B_{Ed}$ (Figure 23b) and $M_{y,Ed} + M_{z,Ed} + B_{Ed}$ (Figure 24b); d) the aluminium I200a section under $M_{y,Ed} + B_{Ed}$ (Figs. 23a, Table 13) and $M_{y,Ed} + M_{z,Ed} + B_{Ed}$ (Figure 24a, Table 13).

Eurocode EN 1993-1-1:2022 [65] offers the possibilty of performing the plastic design of cross-sections with various shapes under the combination of $N_{Ed} + M_{y,Ed}$, $N_{Ed} + M_{z,Ed}$ or $N_{Ed} + M_{y,Ed} + M_{z,Ed}$. The authors identified problems in Eurocode rules related to I-shaped sections under combinations of $N_{Ed} + M_{y,Ed}$ and $N_{Ed} + M_{z,Ed}$, and offer some suggestions about how to solve problems. Instead of approximate Eurocode formulae valid for I-shaped sections under $N_{Ed} + M_{y,Ed}$ combinations, exact formulae (31)-(34) are proposed. Draft prEN 1993-1-1 contains incorrect Mirambell's formula (52) [75] that are valid for I-shaped sections under $M_{y,Ed} + B_{Ed}$ combinations. In Eurocode EN 1993-1-1:2022 [65], Baláž`s formula (54) is applied. Compare them in Figure 22b.

Eurocodes do not offer the possibility of performing plastic designs of channels under the very frequent combination of bending and torsion internal forces $M_{y,Ed} + B_{Ed}$. For this combination, Baláž proposes simple approximate formulae for both: a) positive bimoment B_{Ed} (72) and b) negative bimoment B_{Ed} (70). See Figure 25 or [71]. This proposal was verified by three different computer programmes: a) DUENQ [73], b) QST-TSV-3Blech [74] and c) the interaction diagram in Figure 26 (see also Table 14).

The Appendix presents a detailed example of the very useful MathCad programme by Torsten Höglund for calculating the plastic section modulus of a point symmetric closed oblique cross-section. It can serve as a guide for any other cross-section shape.

Funding: This research project is supported by the Slovak Grant Agency VEGA No. 1/0155/23.

Nomenclature: Eurocode symbols are used.

Appendix A

Example of an *y*-axis plastic section modulus for an oblique hollow section according to Figure 7a)

Cross-section dimensions to the mid of thickness; see Figure A.1

$$h = 34.64mm \qquad b = 50mm \quad c = 20mm \quad t_0 = 0.4mm \qquad o = 0mm \quad \text{(zero)}$$

Webs are not vertical. Therefore, PNAs are inclined. See the dash-dotted line in the figure.

Nodes 0 (6) and 3 should give such values so that the y-coordinate for parts 0-1-2-3 and 3-4-5-6 have the same horizontal gravity centre. This can be achieved by trial and error. See the end of the example.

The PNA in the left web is then found to be $mv = 3.775mm$

The shortened version for web inclination (cotangent) is $ctn = h / c = 1.732$

PNA coordinates mv and $ctm \cdot mv$ give such values so that the gravity centres of the two halves are the same. Due to symmetry, this is in the middle of the section.

Nodes $i = 0..6$ for a coordinate system with the origin in the lower left corner and thicknesses for $i = 0..6$ are:

$$y = \begin{pmatrix} mv \\ c \\ c+b \\ c+b-mv \\ b \\ o \\ mv \end{pmatrix} = \begin{pmatrix} 3.775 \\ 20 \\ 70 \\ 66.225 \\ 50 \\ 0 \\ 3.775 \end{pmatrix} mm \qquad z = \begin{pmatrix} ctn \cdot mv \\ h \\ h \\ h - ctn \cdot mv \\ o \\ o \\ ctn \cdot mv \end{pmatrix} = \begin{pmatrix} 6.538 \\ 34.64 \\ 34.64 \\ 28.102 \\ 0 \\ 0 \\ 6.538 \end{pmatrix} mm \quad t_i = t_0 \tag{A.1}$$

Preprints.org (www.preprints.org) | NOT PEER-REVIEWED | Posted: 6 September 2024 doi:10.20944/preprints202409.0512.v1

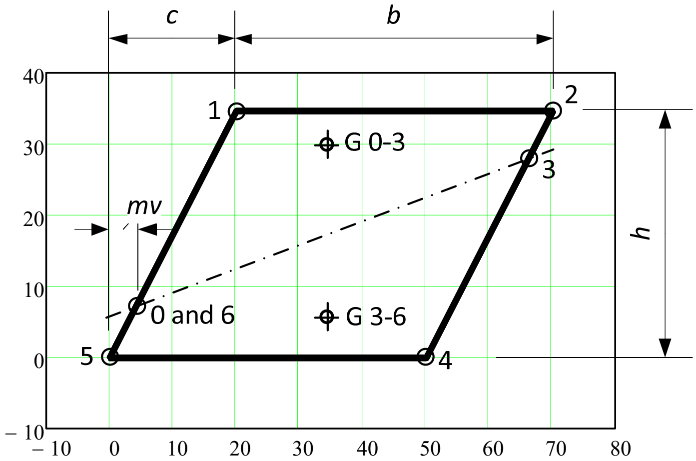

Figure A1. Cross-section of an oblique hollow section.

The plastic section modulus if the PNA is horizontal and in the middle of webs (which is correct for y-axis bending, but only if the beam is laterally restrained all along its length) according to prEN 1999-1-1 Annexe G.10.1, it is $d=\sqrt{h^2+c^2}=40mm$

$$W_{pl,hor}=2t_0 b\frac{h}{2}+2t_0\frac{dh}{4}=970mm^3 \tag{A.2}$$

Firstly check that the cross-section is divided into two equal areas.

The cross-section area of the upper half

$$A_{up}=\sum_{i=1}^{3} t_i\sqrt{(y_i-y_{i-1})^2+(z_i-z_{i-1})^2}=36.0mm^2 \tag{A.3}$$

The cross-section area of the lower half

$$A_{lo}=\sum_{i=4}^{n} t_i\sqrt{(y_i-y_{i-1})^2+(z_i-z_{i-1})^2}=36.0mm^2 \tag{A.4}$$

Set negative t for the lower half, which corresponds to the tension in the lower half.

$$j=4..6 \qquad t_j=-t_j \qquad n=rows(y)-1=6 \tag{A.6}$$

The plastic section modulus according to (G.39)

$$W_{pl,y}=\sum_{i=1}^{n} 0.5t_i\left(z_i+z_{i-1}\right)\sqrt{(y_i-y_{i-1})^2+(z_i-z_{i-1})^2}=863mm^3 \tag{A.7}$$

Compare $W_{pl,hor}=970mm^3$

In Figure A.2, the upper blue part is in compression and the bottom red lower part is in tension.

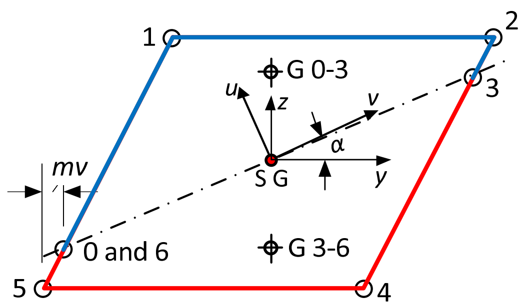

Figure A2. Cross-section divided into two parts.

The following formulae are used to find the horizontally gravity centre in the trial-and-error procedure. When gravity centres are the same, then $mv = 3.775mm$ is found. The areas of all the cross-section parts are:

$$\Delta A_i = t_i \sqrt{\left(y_i - y_{i-1}\right)^2 + \left(z_i - z_{i-1}\right)^2} \tag{A.8}$$

For the upper part, the gravity centre is:

$$y_{G,0-3} = \sum_{i=1}^{re} 0.5\Delta A_i \left(y_i + y_{i-1}\right) \frac{1}{\sum_{i=1}^{re} \Delta A_i} = 35.0mm \tag{A.9}$$

where node $re = 3$ divides the area into two parts.

For the lower part:

$$y_{G,3-6} = \sum_{i=re+1}^{n} 0.5\Delta A_i \left(y_i + y_{i-1}\right) \frac{1}{\sum_{i=re+1}^{n} \Delta A_i} = 35.0mm \tag{A.10}$$

References

1. Kazinczy G. Betonszemle, Vol. 2, p. 68, 1914; also Beton und Eisen, Vol. 32, p. 74–80, 1933.
2. Wikipedia. https://nl.wikipedia.org/wiki/Nicolaas_Christiaan_Kist_(ingenieur).
3. Kurrer K-E. Hermann Maier-Leibnitz (1885–1962): Wegbereiter des Industriebaus der klassischen Moderne. Stahlbau, August 2005; 74(8):623 – 634, DOI: 10.1002/stab.200590137.
4. Maier-Leibnitz H. Beitrag zur Frage der tatsächlichen Tragfähigkeit einfacher und durchlaufender Balkenträger aus St37 und aus Holz. Die Bautechnik, 1928; Heft 1 und 2. Vol. 6, p. 11. Neun Zuschriften: Die Bautechnik, 11. Mai 1928; Heft 20, p. 274-8.
5. Maier-Leibnitz H. Versuche mit eingespannten und einfachen Balken von I-Form aus St37. Bautechnik, 1929; No.20. Stahlbau, 1936; No.20.
6. Wikipedia. https://de.wikipedia.org/wiki/Hans_H._Bleich.
7. Wikipedia. https://en.wikipedia.org/wiki/John_Baker,_Baron_Baker
8. Beedle LS, Thurlimann B, Ketter RL. Plastic design in structural steel. Lecture notes, Summer cours, Lehigh University, AISC; 1955.
9. Fritsche I. Die Tragfähigkeit von Balken aus Stahl mit Berücksichtigung des plastischen Verformungsvermögens. Bauingenieur, 1930. No. 49, 50, 51.
10. Nadai A. Plasticity. New York: McGraw-Hill; 1931.
11. Bleich HH. Über die Bemessung statisch unbestimmter Stahltragwerke unter Berücksichtigung des elastisch-plastischen Verhaltens des Baustoffes. Bauingenieur, 1932. 13(19/20), p. 261–7, Berlin.
12. Eisenmann K. Theorie und Statik plastischer Träger des Stahlbaues. Stahlbau, 1933; H.4.
13. Kann F. Rechnerische Untersuchungen über die Größe des Fließbereiches in stählernen Durchlaufbalken unter Berücksichtigung des Momentenausgleichs. Stahlbau, 1932; No.14, No.20.
14. Abrikosov BG. Analysis of metal structures with plastic deformations (in Russian). ONTI. 1934.
15. Michlin SG. Basic equations of mathematical theory of plasticity (in Russian). Publishing house of AN SSSR; 1934.
16. Gvozdev AA. The determination of the value of the collapse load for statically indeterminate systems undergoing plastic deformation (in Russian). Proc. of the Conf. on Plastic Deformations. Projekt i standard. 1934; No.8.
17. Žudin ND. Analysis of steel structures with plastic deformations (in Russian). Sbornik trudov II. Kijevskij strojiteľnyj institute. Kyiv, Ukraine: GNTI; 1935.
18. Melan E. Die Theorie statisch unbestimmter Systeme aus ideal plastischen Baustoff. S. B. Akad. Wiss. Wien (Abt. IIa) 145, 195. Berlin. 1936.
19. Bezuchov NI. To the theory of the plastic analysis in bending (in Russian). Vestnik inzenerov i technikov 1936; No.10.
20. Colonetti G. Le probléme des déformations plastiques et la theorie des poutres fléchies. Technique des travaux. 1938; No.2.
21. Lejbenzon LS. Elements of mathematical theory of plasticity (in Russian). Gostechizdat. 1943.

22. Volterra E. Results of experiments on metallic beams bent beyond the elastic limit. Journal of the Institution of Civil Engineers. 1943; March Nr.5.
23. Sokolovskij VV. Theory of plasticity (in Russian). Publishing house of AN SSSR; 1946. 2nd edition Moscow: Gostechizdat; 1950.
24. Iľjušin AA. Plasticity (in Russian). Moscow: Gostechizdat; 1948.
25. Van Den Broek JA. Theory of limit design. New York: John Wiley and Sons; 1948.
26. Luxion W, Johnston B. Plastic behaviour of wide flange beams. Welding journal, November 1948; 27(11), p.538. (Progress report #1).
27. Roderick JW. Theory of plasticity – elements of the simple plastic theory. Phil. Mag., July 1948; Series 7, XXXIX, 529.
28. Hrennikoff A. Theory of inelastic bending. Transactions of the American Society of Civil Engineers. January 1948; Volume 113, Issue 1
29. Baker JF. A review of recent investigations into the behaviour of steel frames in the plastic range. Jnl. Inst. Of Civil Engineers, 1949; 3, p. 185-240.
30. Prager W, Hodge PG. Theory of perfectly plastic solids. New York: John Wiley and Sons, Inc.; 1949.
31. Horne MR. Fundamental propositions in the plastic theory of structures. J. Inst. Civ. Engrs., 1950; 34, 174.
32. Nadai A. Theory of flow and fracture of solids. 2nd edition, New York: McGraw-Hill Book Co.; 1950.
33. Symonds PS, Prager W. Elastic-plastic analysis of structures subjected to loads varying arbitrary between prescribed limits. J. appl. Mech., 1950; 17, p. 315-332.
34. HILL R. The Mathematical Theory of Plasticity. London: Oxford University Press; 1950.
35. Bezuchov NI. Introduction in theory of elasticity and plasticity (in Russian). Strojizdat; 1950.
36. Symonds PS, Neal BG. Recent progress in the plastic methods of structural analysis. Journal of Franklin Inst., November, 1951; 252(5), p. 383-407 and December, 1951; 252(6), p. 469-492.
37. Greenberg HJ, Prager W. On limit design of beams and frames. ASCE. February 1951; Separate No. 59.
38. Baldin VA, Goľdenblat II. Investigations of limit states of civil engineering structures (in Russian). Gosstrojizdat; 1951.
39. Yang CH, Beedle, LS. Plastic design and deformation of structures. Welding journal, July 1951; 30(7), p.348, (January 1952, with discussion by Symonds 31(1), p.33).
40. Broude BM. Limit state of steel beams (in Russian). Gosstrojizdat; 1953.
41. Bezuchov NI. Theory of elasticity and plasticity (in Russian). Moscow: GITL; 1953.
42. Hoffman O, Sachs G. Introduction to the theory of plasticity for engineers. New York-Toronto-London: McGraw Hill; 1953.
43. Johnston B, Yang CH, Beedle LS. An evaluation of plastic analysis as applied to structural design. Welding journal, 1953; 32(5), p. 225-232. (Progress report #8).
44. Ržanicyn AR. Analysis of structures with plastic properties of materials (in Russian). Moscow: Gostechizdat; 1954.
45. Horne MR. A moment distribution method for the analysis and design of structures by the plastic theory. Inst. Of Civil Engineering. April 1954; Proc. p.51.
46. Sobotka Z. Theory of plasticity and limit states of civil engineering structures I., and II. (in Czech). Prague: Publishing house of ČSAV; 1954 and 1955.
47. Prager W. Probleme der Plastizitätstheorie. Basel – Stuttgart: Birkhäuser; 1955.
48. Prager W. The Theory of Plasticity: A Survey of Recent Achievements. Proceedings of the Institution of Mechanical Engineers. June 1. 1955; Volume 169, Issue 1.
49. Kačanov AM. Basis of theory of plasticity (in Russian). Moscow: GITL; 1956.
50. Neal BG. The plastic methods of structural analysis. London: Chapman and Hall; 1956.
51. Baker JF, Horne MR, Heyman J. The steel skeleton II. Plastic Behaviour. Cambridge: Cambridge University Press; 1956.
52. Drucker DC. Plastic design methods – advantages and limitations. Transactions, Soc. nav. Arch. mar. Engrs. 1958; 65.
53. Streľbickaja AI. Investigation of resistance of thin-walled columns behind yield strength (in Russian).. Kyiv: Publishing house of AN USSR; 1958.
54. Hodge PhG. Plastic analysis of structures. New York-Toronto-London: McGraw Hill; 1959.
55. Commentary on plastic design in steel. Chapter 5. Journal of the Engineering Mechanics Division. Proceedings of the AISC. EM 3, 1959.
56. Massonet Ch, Save, M. Calcul plastique des constructions. Bruxelles: Édité par le Centre Belge – Luxembourgeois d`Information de l`Acier; 1961.
57. Massonnet Ch, Olszak W, Phillips A. Plasticity in Structural Engineering, Fundamentals and Applications. Wien: Springer-Verlag; 1979.
58. Mrázik A, Škaloud M, Tocháček M. Plastic Design of Steel Structures. Chichester and Prague: Ellis Horwood Limited; 1986.

 doi:10.20944/preprints202409.0512.v1

59. Kindmann R, Frickel J. Grenztragfähigkeit von häufig verwendeten Stabquerschnitten für beliebige Schnittgrößen. Stahlbau 1999, 68, p. 817–828. [CrossRef].
60. Kindmann R, Frickel J. Elastische und Plastische Querschnittstragfähigkeit Grundlagen, Methoden, Berechnungsverfahren, Beispiele. Mit CD-ROM: RUBSTAHL Lehr- und Lernprogramme.: Berlin: Ernst & Sohn, Wiley Company; 2002.
61. Osterrieder P, Kretzschmar J. First-hinge analysis for lateral buckling design of open thin-walled steel members. J. Constr. Steel Res. 2006; 62, p. 35–43. [CrossRef].
62. Vayas I. Interaktion der plastischen Grenzschnittgrößen doppelsymmetrischer I-Querschnitte. Stahlbau 2000; 69, p. 693–706. [CrossRef].
63. Vayas I, Charalampakis A, Koumousis, V. Inelastic resistance of angle sections subjected to biaxial bending and normal forces. Steel Construction 2 (2009); No. 2.
64. Baláž, I. Slovak National Annex to STN EN 1993-1-1:2024. ÚNMS SR Bratislava.
65. EN 1993-1-1:2022 Eurocode 3: Design of Steel Structures. Part 1-1: General Rules and Rules for Buildings. CEN Brussels.
66. EN 1993-1-1:2005 Eurocode 3: Design of Steel Structures. Part 1-1: General Rules and Rules for Buildings. CEN Brussels.
67. EN 1999-1-1:2023 Eurocode 9: Design of Aluminium Structures. Part 1-1: General Structural Rules. CEN Brussels.
68. EN 1999-1-1:2007 Eurocode 9: Design of Aluminium Structures. Part 1-1: General Structural Rules. CEN Brussels.
69. Baláž I.: Slovak comments to prEN 1993-1-1. Sent to CEN/TC250 SC3 WG1 20.11.2020. ÚNMS SR Bratislava.
70. Gardner L. The Continuous Strength Method for Steel, Stainless Steel and Aluminium Structural Design, Proceedings of the Eight International Conference on Steel and Aluminium Structures, December 7.-9.2016, Hong Kong, China.
71. Baláž I. Koleková Y. Resistances of I- and U-Sections. Combined Bending and Torsion Internal Forces. Eurosteel 2017, September 13–15, 2017, Copenhagen, Denmark. Paper No. 13_12_ 772 on USB, pp. 1-10.
72. Baláž I, Koleková Y. Plastic Resistance of I- and U-section under Bending and Torsion. In: Institut für Konstruktion und Entwurf Universität Stuttgrat. Stahlbau, Holzbau und Verbundbau. Festschrift zum 60. Geburtstag von Univ.-Prof. Dr.-Ing. Ulrike Kuhlmann. Berlin: Ernst & Sohn. A Wiley Brand; 2017, p. 203-209.
73. Dlubal Software GmbH, Programm DUENQ (SHAPE-THI) 8.07.03.185540 x32, 2016.
74. Wolf Ch. Frickel J. Programm QST-TSV-3Blech, Ruhr-Universität Bochum.
75. Mirambell E, Bordallo J, Real E. Torsion and its interaction with other internal forces in EN 1993-1-1 – a new approach, Steel Construction, 2016; No. 3, p. 240-248.
76. Baláž I, Kováč M, Živner T, Koleková Y. Plastic resistance of H-section to interaction of bending moment $M_{y,Ed}$ and bimoment B_{Ed}. Proceedings of the 2nd International Conference on Engineering Sciences and Technologies, High Tatras Mountains, Tatranské Matliare, Slovak Republic. Leiden, Netherlands: CRC Press, Taylor & Francis Group, A Balkema book, 2017, p. 33-38.
77. Baláž I, Kováč M, Živner T, Koleková Y. Plastic resistance of IPE-section to interaction of bending internal forces $M_{y,Ed}$, $V_{z,Ed}$ and torsion internal forces B_{Ed}, $T_{\omega,Ed}$ and $T_{t,Ed}$. Proceedings of the 2nd International Conference on Engineering Sciences and Technologies, High Tatras Mountains, Tatranské Matliare, Slovak Republic. Leiden, Netherlands: CRC Press, Taylor & Francis Group, A Balkema book, 2017, p. 27-32.